

1 **Revision 4: Compositional variation and timing of aluminum phosphate-sulfate minerals in**
2 **the basement rocks along the P2 fault and in association with the McArthur River uranium**
3 **deposit, Athabasca Basin, Saskatchewan, Canada**

4 Erin E. Adlakha and Keiko Hattori

5 Department of Earth Sciences, University of Ottawa, Ottawa, ON, K1N6N5, Canada. E-mail:
6 eadla028@uottawa.ca

7 **Abstract**

8 The Athabasca Basin hosts world class uranium deposits, such as the McArthur River
9 deposit. This paper presents the occurrence of aluminum phosphate-sulfate (APS) minerals in the
10 metasedimentary rocks along the P2 fault, the main ore-hosting fault of the McArthur River
11 deposit. It compares the APS minerals along the P2 fault with those outside the fault, examined in
12 this study, and those from other deposits of the Athabasca Basin and from other Paleo- to
13 Mesoproterozoic basins worldwide.

14 APS minerals are common along the P2 fault, rare outside of the P2 fault zone in the
15 basement, and sparse along the unconformity between the Athabasca sandstones and the
16 basement. The APS minerals along the P2 fault occur with sudoite (\pm illite, magnesiofoitite) and
17 are zoned with Sr-, Ca- and S-rich cores (solid solution between svanbergite, crandallite and
18 goyazite) and LREE- and P-rich rims (close to florencite composition). APS minerals in the
19 Bleached Zone (altered rocks along the unconformity consisting predominantly of kaolin and
20 illite) are Sr-, Ca- and S-rich (high svanbergite component) and occur with kaolin. APS minerals
21 in the Red-Green Zone (mingled red hematitic and green chloritic basement rocks below the

22 Bleached Zone) occur with sudoite and clinochlore. They contain relict cores of LREE- and As-
23 rich arsenoflorencite-(Ce), and rims of svanbergite-goyazite-crandallite solid solution.

24 The occurrence of svanbergite-crandallite-goyazite along the unconformity suggests their
25 formation by relatively oxidizing fluids during diagenesis of the overlying sandstones. The relict
26 cores of arsenoflorencite-(Ce) in the Red-Green Zone are interpreted to be the product of paleo-
27 weathering before the deposition of the Athabasca sandstones. Florencitic APS minerals are
28 found along the entire studied strike length (7 km) of the P2 fault, including the ore zone and
29 non-mineralized areas, but absent outside the fault zone. The florencitic APS minerals contain
30 low SO_4^{2-} in the ore zone, suggesting relatively reducing conditions during their crystallization.
31 Zoned APS minerals (with svanbergitic cores and florencitic rims) proximal to ore contain
32 elevated U (up to 16 ppm). These features suggest that diagenetic, oxidizing, and uranium-
33 bearing fluids travelled along the P2 fault and became relatively reduced, especially within the
34 ore zone. It also suggests florencitic APS minerals are contemporaneous with uranium
35 mineralization. The restricted occurrence of florencitic APS mineral along the P2 fault in the
36 basement suggests their use in identifying fertile basement structures associated with uranium
37 mineralization.

38 *Keywords:* hydrothermal alteration, APS, uranium mineralization, florencite, svanbergite,
39 arsenoflorencite, diagenesis, paleo-weathering, unconformity-type uranium deposits

40 **Introduction**

41 The Athabasca Basin hosts numerous large uranium deposits (Fig. 1), which are classified
42 as unconformity-related uranium deposits. The prevalent model for the mineralization was first
43 proposed by Hoeve and Sibbald (1978) and modified later by many researchers (e.g. Alexandre et

44 al. 2005; Derome et al. 2005; Richard et al. 2011; Mercadier et al. 2012). This model suggests
45 that sea-water derived, uranium-bearing oxidizing brines (25-35 wt.% eq. NaCl) precipitated
46 uranium ore at the unconformity when it reacted with a reducing fluid of currently unknown
47 origin. Many deposits occur in the proximity of deformation zones in the basement and it is
48 suggested that re-activated basement faults served as conduits for uranium-bearing fluids
49 (Jefferson et al. 2007) or reducing basement fluids to reach the unconformity (McGill et al.
50 1993). The McArthur River deposit, the largest discovered high-grade (average grade of 16.46
51 %U₃O₈; Bronkhorst et al. 2012) uranium deposit on Earth, is situated along the P2 fault, a 13 km
52 long reverse fault constrained to graphitic metapelite below the Athabasca Basin. Although
53 geophysical and structural studies have been carried out on the P2 fault (e.g., Hajnal et al., 2010),
54 the exact role of the fault in the mineralization remains uncertain.

55 In the Athabasca and Thelon basins of Canada, aluminum phosphate-sulfate (APS)
56 minerals (also known as alumino-phosphate sulfate) spatially associated with uranium deposits
57 have been reported (Quirt et al. 1991, Gaboreau et al. 2007, Riegler et al. 2014). APS minerals
58 occur in a variety of environments (Dill, 2001) and form many solid solution series with over 40
59 end-members (Jambor 1999; Stoffregen et al. 2000; Dill 2001). APS minerals have the general
60 formula: AB₃(XO₄)₂(OH)₆, where A = mono-, di-, tri- or, more rarely, tetravalent cations (K⁺,
61 Na⁺, Rb⁺, Ca²⁺, Sr²⁺, REE³⁺, Th⁴⁺ etc.); B = trivalent cations (Al³⁺, Fe³⁺); and X = P⁵⁺, S⁶⁺, or
62 As⁵⁺. Since incorporation of ions with different valences requires coupled substitution to
63 accommodate charge balance, compositional zoning of APS minerals is commonly well
64 preserved. This makes APS minerals excellent candidates for evaluating the chemical and
65 physical characteristics of fluids from which they formed (Dill 2001; Beaufort et al. 2005;
66 Gaboreau et al. 2005, 2007).

89 discussion. Macdonald (1985) considered them as the products of paleo-weathering before
90 sandstone deposition, whereas Cuney (2003) proposed their formation after the deposition of
91 sandstones. Quirt (2001) and Adlakha et al (2014) pointed out extensive overprinting of alteration
92 minerals by subsequent hydrothermal fluids, which makes it difficult to determine the condition
93 of their initial crystallization. Rocks of the Bleached Zone are altered to white due to loss of
94 hematite and interpreted to be a reaction product of the Red Zone with late diagenetic fluids from
95 the overlying basin (Macdonald 1985; Quirt 2001). The least-altered metapelite occurs > 50 m
96 below the unconformity and away from faults.

97 The sedimentary rocks of the Athabasca Group are comprised of dominantly fluvial to
98 shallow marine, quartz pebble conglomerate and quartz arenite, with a preserved maximum
99 thickness of 1500 m in the centre of the basin (Ramaekers et al. 2007). Early diagenesis included
100 silica cementation on hematite-dusted detrital quartz grains (Hoeve and Quirt 1984; Jefferson et
101 al. 2007), alteration of kaolinite by dickite with minor illite and locally traces of sudoite (Quirt
102 2001; Laverret et al. 2006). Uranium deposits are localized near the intersection of the
103 unconformity and basement faults or down-dip along these faults into the basement. These
104 deposits are surrounded by alteration haloes of sudoite, illite and magnesio-foitite (alkali-
105 deficient dravite). Sandstone-hosted unconformity-type deposits show the inner halo of sudoite
106 with an outer alteration halo of illite (e.g., Hoeve et al. 1981; Hoeve and Quirt 1984; Alexandre et
107 al. 2012). Basement-hosted unconformity-type deposits are accompanied by the inner alteration
108 halo of illite and the outer halo of sudoite. The different proportions of sudoite and illite between
109 two types of unconformity-type deposits are considered to be related to differences in fluid
110 circulation (i.e. Ingress vs Egress; Hoeve and Quirt 1984).

111 **Structure and alteration of the McArthur River deposit and P2 fault**

112 The McArthur River deposit is comprised of six ore bodies, Zones 1-4 and Zones A and
113 B, which collectively have a strike length of approximately 1.7 km near the intersection of the P2
114 fault (~050°/45-60°) and the unconformity, ~500 m below surface (Fig. 2c) (McGill et al. 1993;
115 Alexandre et al. 2005; Bronkhorst et al. 2012). The total reserves of the McArthur River deposit
116 as of August 31, 2012, were 385.5 Mlbs U₃O₈ (Bronkhorst et al. 2012). All ore bodies are hosted
117 in the sandstone immediately above the unconformity except for the Zone 2 ore body which
118 occurs immediately below the unconformity and is bounded by the vertical quartzite (VQ) fault
119 and ~140° trending series of cross faults (Fig. 2b). Late minor remobilizations of uraninite
120 formed veinlets and fractures with pyrite, chalcopyrite and minor nickel-cobalt sulfarsenides
121 (McGill et al. 1993).

122 The P2 fault zone is a series of reverse faults with a strike length of approximately 13 km
123 (McGill et al. 1993) and has been traced seismically at least 2 km below the unconformity
124 (Hajnal et al. 2010). In the basement, the several fault planes of the P2 fault are mostly
125 constrained to graphite-bearing metapelite and trend parallel to the basement foliation (McGill,
126 1993). Reactivation of P2 faulting formed differences in the thickness of the basal conglomerate
127 at the unconformity and broad fracture and breccia zones in the sandstones and the reverse
128 movement of the P2 fault raised a wedge of basement rocks above the unconformity with the
129 vertical displacement of up to 80 m (McGill et al. 1993; Figs. 2a,b). The basement wedge is also
130 referred to as the “middle block” by workers (Bronkhorst et al. 2012) as it is offset by differential
131 movement of fault planes (Figs 2a,b). These offsets at the apex (or the “nose”) commonly hosts
132 the uranium mineralization of McArthur River deposit and sporadic occurrences of low-grade (<1
133 %U₃O₈) mineralization along the P2 fault (Fig. 2a). The P2 fault and basement rocks show minor

134 lateral displacement by three sets of steeply dipping faults that strike $100 - 110^\circ$ in the mine-site
135 area (Fig. 2b). These faults and offsets likely provided pathways for mineralizing fluids, but also
136 truncate high-grade zones, especially the Zone 2 ore body (Fig. 2b; McGill et al. 1993;
137 Bronkhorst et al. 2012).

138 Basement rocks along the P2 fault were intensely altered to form sudoite, illite, magnesio-
139 foitite, Fe-Mg chlorite, and sulfides (McGill et al. 1993; Adlakha et al. 2014). The hanging wall
140 basements rocks, including the ore-hosting wedge, commonly show intense alteration forming
141 sudoite and illite \pm kaolin. Formation of illite and/or kaolin makes rocks creamy white in colour,
142 and this alteration is called “bleaching”. Bleaching is common, especially in close proximity to
143 the fault, mineralization and the unconformity (McGill et al. 1993). The most intense alteration of
144 the basement rocks is found in close proximity to the Zone 2 ore body where sudoite and
145 magnesiofoitite are the dominate alteration minerals (Adlakha et al. 2014). In comparison, illite
146 with minor sudoite are the dominate alteration minerals in the moderately altered basement rocks
147 in unmineralized areas (the south-west portion of the P2 fault) and near the weakly mineralized
148 P2 Main deposit (Fig. 2b), that is “perched” higher in sandstones. APS minerals only occur in
149 highly altered rocks where primary metamorphic minerals and textures are altered.

150

Sampling

151 A total of 192 samples of metasedimentary rocks, predominately metapelites with fewer
152 pegmatite and quartzite, were collected from 27 different drill-holes along the P2 fault zone from
153 the McArthur River mine site to ~ 7 km southwest (Fig. 3). Of these, 139 samples were selected
154 for examination of APS minerals in thin sections. Out of the 139 samples, APS minerals were
155 found in only 17 samples. Among these 17 samples, APS minerals in 4 samples were too small
156 for quantitative analysis with electron microprobe analyzer (EPMA). Of these remaining 13

157 samples (Table 1), nearly all were from metapelites located along the P2 fault (11 of 13) that
158 showed intense/pervasive alteration in which clay-sized minerals replaced most metamorphic
159 minerals and metamorphic textures were obliterated by alteration, fractures and/or veinings. In
160 this paper, samples collected within 50 m of the centre of the fault are considered to be associated
161 with P2 fault, as the fault is accompanied by splay structures and alteration extending outside the
162 fault zone.

163 The samples associated with the P2 fault were collected from varying distances to the
164 McArthur River uranium deposit (Fig. 2c; Table 1). MAC425 was collected within the Zone 2
165 ore body (Fig. 3A), MAC152 < 15 m from the Zone 2 ore body, MAC67 (Fig. 3b) and MAC85 <
166 20 m from the Zone 2 ore body, MAC63 < 50 m from the Zone 2 ore body, MAC43 and MAC44
167 <50 m from the Zone 3 ore body. MAC29 was within 1 m of low grade (< 1 wt% U₃O₈) uranium
168 mineralization disseminated within the sandstone (Fig. 2a), MAC404 was approximately 50 m
169 from low grade uranium mineralization within the sandstone. MAC117 and MAC35 are >500 m
170 away from low grade uranium mineralization in the sandstone, >1 km from the low grade P2
171 Main deposit and > 2 km from the McArthur River deposit.

172 Although 5 samples from the Bleached Zone were examined in detail, APS minerals were
173 found only in one sample (MAC17; Fig. 3c) of quartzite along the unconformity, > 250 m from
174 low grade mineralization and > 1 km from the McArthur River deposit (Fig. 2a,c). Twenty-two
175 samples of metasedimentary rocks of the Green, Red-Green and Red Zones outside the P2 fault
176 were examined and APS minerals were found only in one sample (MAC412) of strongly
177 hematized and chloritized metapelite from the Red-Green Zone in the footwall near the P2 Main
178 deposit (Figs. 2c, 3d). Here we use field terminology “Bleached Zone” and the “Red-Green
179 Zone” to reflect the samples position within the basement rocks as these terms were commonly

180 used by geologists in the area. The Bleached Zone occurs along the unconformity and it refers to
181 a creamy-white colored zone where kaolin and illite predominate. The Red-Green Zone is a
182 physical mixture of hematitic Red Zone and chloritic Green Zone.

183 **Methods**

184 Thin sections were examined using an optical petrographic microscope with reflected and
185 transmitted light sources. Due to the very fine-grained nature of minerals in the samples, detailed
186 textural analysis was also carried out on carbon-coated polished thin sections using a JEOL
187 6610LV scanning electron microscope (SEM) at the University of Ottawa. Minerals were
188 identified using energy-dispersive spectroscopy with the spectrum acquisition time of 40 s and an
189 accelerating voltage of 20 kV.

190 Quantitative analysis for the major and minor elemental compositions of the APS
191 minerals was carried out using a JEOL 8230 EMPA at the University of Ottawa. APS minerals
192 were analyzed at an accelerating voltage of 15 kV, a beam current of 20 nA using a focused beam
193 of 5 μm (to account for alkali migration). Counting times were 20s on-peak and 10s off-peak for
194 all elements except for S (10s on and 5 s off), F (50s on and 25s off), Pr (20s on and 5s off) Cl
195 (25s on 12s off), P (10s on and 5s off), Si (10s on and 5s off) and As (20s on and 20 s off). The
196 mineral standards used were sanidine (Si, Al, K), hematite (Fe), apatite (Ca, P, F), albite (Na),
197 tugtupite (Cl), celestine (Sr, S), synthetic NdPO_4 (Nd), PrPO_4 (Pr), CePO_4 (Ce), LaPO_4 (La),
198 ThO_2 (Th) and GaAs (As). The elemental concentrations were calculated after matrix interference
199 correction using ZAF. Elemental maps of selected APS grains were acquired at an accelerating
200 voltage of 10 kV with a 10 nA current at a counting time of 0.5 s per pixel with a total of 10000
201 pixels per image.

202 APS minerals are small (mostly < 20 μm , rarely up to 40 μm) and surrounded by quartz
203 and fine-grained alteration minerals (Fig. 4; Table 1-2), but it was necessary to use a broad
204 electron beam of 5 μm to minimize the loss of alkalis from APS minerals during the EPMA
205 analysis. This made it unavoidable for the surrounding minerals to contribute to the analytical
206 results. To evaluate the possible contributions of surrounding minerals in the chemical
207 composition obtained for the APS, their compositions were measured by EMPA. The contents of
208 SiO_2 were used to monitor the contribution of surrounding minerals because APS minerals rarely
209 contain Si. For the data showing Si, the amounts of K, Al, and Na of the surrounding phases were
210 subtracted from the analytical results. For example, for Al_2O_3 using the equation, $\text{Al}_2\text{O}_{3\text{APS}}$
211 $\text{corrected} = \text{Al}_2\text{O}_{3\text{APS analyzed}} - (\text{SiO}_{2\text{APS analyzed}} * \text{Al}_2\text{O}_{3\text{matrix}} / \text{SiO}_{2\text{matrix}})$. The remaining concentration
212 values were normalized to the original analytical total. Table 2 shows the contents of SiO_2 before
213 subtracting the contribution of surrounding minerals. The contribution of surrounding minerals
214 never exceeded 5% of the total.

215 Trace element contents in the APS minerals were determined using polished thick (>60
216 μm) sections by laser ablation inductively coupled plasma mass spectrometer (LA-ICP-MS) at
217 the Geological Survey of Canada, Ottawa, using a Photon-Machines Analyte193 ArF excimer
218 laser ($\lambda = 193 \mu\text{m}$) with Helex ablation cell and Agilent 7700x quadrupole ICP-MS. Helium gas
219 was used to transport ablated sample from the ablation cell and was mixed with Ar plasma (flow
220 rate of 1.05 mL/min) via a T-connector before entering the ICP. The detailed operating
221 conditions for the LA-ICP-MS instrument and the isotopes quantified are listed in Appendix
222 Table 1. During analysis, ~40 s of background signal with the laser turned off was collected and
223 then ablation was performed by a laser focused to 10 μm for a data acquisition time of ~60 s
224 (total time of 100 s for one analysis) for a total time of 100 s for one analytical cycle. The isotope

225 counts were monitored during the analysis, and the acquisition time for the data of APS minerals
226 was adjusted (Appendix Fig. 1). Aluminum contents are similar among grains of APS minerals.
227 Therefore, the counts of these isotopes and their count ratios to Al in the sample and the reference
228 NIST610 (National Institute of Standards and Technology) were used to calculate the element
229 abundances (Longerich et al. 1996). There is no international standard that has the composition
230 similar to APS minerals. Therefore, the standard NIST610 was used as it contains high Al and it
231 is the most used standard. The elemental concentrations were obtained based on the count ratios
232 of elements to Al and the average Al contents in APS minerals of the sample determined by
233 EMPA (Table 2). The Al content was used because Al does not vary between the core and rim of
234 APS minerals (Table 2). The same grains could not be analyzed both by EPMA and LA-ICP-MS
235 because electron beam decomposes APS minerals (Appendix Fig. 2). EMPA and LA-ICP-MS
236 data is comparable (Appendix Fig. 3). One round of LA-ICPMS analysis consisted of seven
237 analyses of grains, bracketed by two analyses of the NIST610 reference and one analysis of the
238 BCR2G (Basalt, Columbia River) reference from USGS. The analysis of NIST610 shows that a
239 counting precision of > 98 % for all elements. Accuracy, determined by BCR2G, was > 90 % for
240 all elements except for Sc, Ti, Fe, Zn, Ce, Pr, Sm, Ho, Lu, Gd, Tb, Pb and Th which were > 85 %
241 and Cu, Y, Zr, Cr, Tm, Yb and Hf which were > 75%.

242

Results

243 Mineral occurrence and distribution

244 APS minerals were found in metapelites along the 7 km section of the P2 fault examined
245 (Fig. 2). APS minerals were found only in one sample from the Bleached Zone (sample MAC17
246 in quartzite) (Figs. 2a, 4i; Table 1). APS minerals are rare in the basement rocks distal from the

247 unconformity and outside the P2 fault. They were found in only one sample (sample MAC 412)
248 in metapelite that contains hematite and chlorite alteration (Fig. 3d) in the footwall 100 m from
249 the P2 fault, 50 m below the unconformity and 100 m away from uranium mineralization (Fig.
250 4h; Table 1). APS minerals were not observed in samples along the VQ fault (Fig. 2b) or in
251 samples of the least-altered basement rocks.

252 APS minerals along the P2 fault occur together with fine-grained sudoite and/or illite
253 intergrown with magnesiofoitite (Adlakha et al. 2014; Figs. 4a-f). Less commonly, APS minerals
254 occur with kaolin and illite, or a mixture of clinochlore and sudoite. In the Bleached Zone
255 sample, APS minerals occur with kaolin and illite (Fig. 4i). APS minerals are rare in the
256 transitional Red-Green Zone and occur predominately with clinochlore (Fig. 4h).

257 APS minerals are small (mostly < 20 μm , rarely up to 40 μm), transparent, pseudo-cubic
258 (rarely hexagonal) crystals, disseminated and/or clustered in fine-grained clay minerals (Fig. 4).
259 There is no evidence of dissolution between APS minerals and surrounding clay minerals. The
260 texture suggest that they are in equilibrium (Figs. 4a-j,l). APS minerals are commonly zoned.
261 Zoning may be observed using plane polarized light microscopy as some cores show high relief.
262 SEM BSE-images commonly show darker cores with lighter rims (Fig. 4c), although grains with
263 lighter cores and darker rims are also observed (Fig. 4h). Darker parts in BSE images are due to
264 greater amounts of Sr and Ca, and brighter parts contain higher LREE.

265 In all samples, APS minerals commonly occur in contact and/or are spatially associated
266 with zircon (Figs. 4f,g), primary apatite (Fig. 4l), or sulfide minerals, such as pyrite (Fig. 4k) and
267 lesser chalcopyrite (Fig. 4d). Zircon grains associated with APS minerals are commonly fractured
268 and/or partially dissolved and rimmed by xenotime (cf. Quirt et al. 1991) (Fig. 4g). Apatite forms

269 subhedral, rounded crystals and APS minerals also occur with small hydrothermal fluorapatite
270 crystals as disseminations or clusters. APS minerals commonly contain inclusions of sulfides or
271 Fe-oxide (Figs. 4h,k,l). APS minerals in the Zone 2 ore body are in close proximity (within the
272 same thin section) with uraninite.

273 **APS mineral chemistry – major elements**

274 The APS mineral formulae were calculated based on 6 cations (Table 2) as the ideal
275 formula is expressed as $AB_3(XO_4)_2(OH)_6$, where A = mono-, di-, tri- or, more rarely, tetravalent
276 cations (K^+ , Na^+ , Rb^+ , Ca^{2+} , Sr^{2+} , REE^{3+} , Th^{4+} etc.); B = Al^{3+} , Fe^{3+} ; and X = P^{5+} , S^{6+} , and As^{5+} .
277 Cation charges were allocated using the following:

- 278 i. the X-site was filled with P^{5+} , S^{6+} , As^{5+} ,
- 279 ii. the B-site was filled by Al^{3+} , then Fe^{3+} to have 3 cations,
- 280 iii. the A site was then filled by remaining cations.

281 High contents of trivalent cations in the A site create excess cation charges. To compensate for
282 this, $PO_3(OH)^{2-}$ is assigned for $(PO_4)^{3-}$, as has been used by previous researchers (e.g., Gaboreau
283 et al. 2007).

284 Along the P2 fault, APS minerals occur predominately with sudoite and lesser illite and
285 magnesiofoitite, in intensely altered metapelite and pegmatite. These APS minerals contain high
286 $\Sigma LREE$ (0.35 – 0.58 apfu; $LREE = La + Ce + Pr + Nd$) relative to Sr (0.16 – 0.32 apfu) and Ca
287 (0.18 – 0.28), and high PO_4^{3-} (1.70 - 1.97 apfu) relative to SO_4^{2-} (0.06 – 0.35 apfu) and AsO_4^{3-}
288 (<0.01 apfu) (Table 2). Ce is high (0.15 – 0.27 apfu) relative to La (0.09 – 0.17), Pr (<0.01 – 0.03
289 apfu), producing $[Ce]_N / [Ce]_N^*$ of ~0.8 – 1.6, where $[Ce]_N^* = \sqrt{([La]_N [Pr]_N)}$. Cores of zoned
290 grains are enriched in Sr-, Ca-, and S, and rims contain high LREE and P (Fig. 5a; Table 2).

291 Within the cores, Ca and P contents are inversely correlated with Sr and S contents (Fig. 5a).
292 Narrow width of zoning and small size of grains prevented acquisition of quantitative
293 compositions of individual zones excluding coarse grains in MAC152 (Table 2). Therefore, most
294 data presented in Table 2 represents mixtures (referred to as mixed data) of compositional zones
295 identified in SEM-BSE.

296 APS minerals in the sample of Bleached Zone quartzite (sample MAC17) contain high Sr
297 (0.68 apfu) relative to Ca (0.16 apfu) and Σ LREE (0.13 apfu) and high SO_4^{2-} (0.54 apfu; Table 2).

298 APS minerals are abundant in the Red-Green Zone sample of the basement footwall
299 (MAC412) near the P2 Main deposit. APS minerals occur with clinocllore and sudoite and
300 contain high AsO_4^{3-} , (~ 0.63 apfu), Fe^{3+} (0.16 apfu), and Ce (~0.32 apfu) showing positive Ce
301 anomalies ($[\text{Ce}]/[\text{Ce}]^*$) of up to 6. APS minerals from this sampl are also zoned with high-Ce
302 cores, and a Ca- and P-rich inner rim and Sr-rich outer rim (Fig. 5b). APS minerals in this sample
303 were relatively coarse-grained; therefore, individual core and rims were analyzed in two grains
304 (Table 2). The data shows that the cores contain high As (0.78 apfu) and low P (0.92 apfu)
305 relative to the rim (0.26 and 1.46 apfu, respectively; Table 2).

306 **APS mineral chemistry – trace elements**

307 LA ICP-MS analyses were conducted on relatively coarse-grained (>10 μm) APS
308 minerals proximal to the Zone 3 (sample MAC44) and Zone 2 ore deposits (samples MAC63 and
309 MAC85). Counts of all elements were monitored during the analysis to detect mineral inclusions
310 and contributions of surrounding minerals. Mineral inclusions should give sharp increases in the
311 counts of elements, but no such spikes were observed during the analysis, confirming the lack of
312 mineral inclusions. None of surrounding minerals contain any significant concentrations of

313 elements described below. Counts of elements, such as U, Y, Pb and Th were at background
314 levels in surrounding minerals and only high when the laser beam hit APS grains. Unlike clays,
315 APS minerals show high counts of LREE, Sr, Ca and P (Appendix Fig. 1). This confirms that
316 these elements are in the APS crystal structure and were not incorporated from surrounding
317 minerals. Furthermore, different grains from individual sections yielded comparable
318 concentrations of minor and trace elements, suggesting that these trace elements originate from
319 APS minerals and that the values are minima since the dilution effects by the surrounding
320 minerals were not corrected. The dilution effects by surrounding minerals are confirmed by the
321 detection of a significant Si (48000 – 99000 ppm) during the ablation of the APS minerals.

322 APS minerals in P2 fault proximal to Zone 3 (MAC44) ore deposit contain appreciable Se
323 (130 ppm), U (0.39 – 0.88 ppm), Pb (160 - 180 ppm), and Th (1100 - 1600 ppm). Similarly, APS
324 from sample MAC63 (~50 m) from Zone 2 ore and ~ 20 m into the hanging-wall of the P2 fault)
325 show appreciable Se (100 – 160 ppm), U (1.7 – 4.2 ppm), Pb (82 – 190 ppm), and Th (1000 –
326 1400 ppm). Sample MAC85, from within 20 m of Zone 2 ore and directly within the P2 fault,
327 contains APS with relatively high U (16 ppm), Pb (260 ppm), and Th (2300 ppm); this sample
328 also contains high LREE (0.54 apfu; Table 2). Similar to samples MAC44 and MAC63, sample
329 MAC85 showed appreciable Se (130 ppm). Combined with the EPMA data of major elements
330 (La, Ce, Pr, Nd), these APS minerals from the P2 fault area contain high LREE relative to HREE
331 ($[\text{LREE}]_{\text{N}}/[\text{HREE}]_{\text{N}} = 800 - 2500$; Fig. 6) and show low S/Se weight ratios, ranging from 100 –
332 150.

333

Discussion

334 Major element compositions of APS minerals

335 The following elemental relationships are observed:

- 336 i. the P contents positively correlate with LREE and both inversely correlate with Sr and S
337 (Figs. 5a, 7c,d); the LREE inversely correlate with Ca (Figs. 5a, 7d);
- 338 ii. the S contents positively correlate with Sr and inversely correlate with Ce (Figs. 5a, 7b).
- 339 iii. high Ca correlates with high P (Figs. 5a,b);
- 340 iv. the As contents inversely correlate with P;
- 341 v. high As APS minerals contain high Ce relative to other REE (Fig. 7a).

342 The above relationships and cations in A-site and X-site (Fig. 8) suggest the presence of the
343 following end-members:

- 344 i. high LREE and P contents correspond to high proportions of florencite
345 $(\text{REE})\text{Al}_3(\text{PO}_4)_2(\text{OH})_6$ (Figs. 8a-c);
346 high S and Sr contents correspond to high proportions of svanbergite $\text{SrAl}_3(\text{PO}_4)(\text{SO}_4)(\text{OH})_6$ with
347 a minor goyazite component $\text{SrAl}_3(\text{PO}_4)_2(\text{OH})_6$ (Figs. 8a-d);
- 348 ii. high Ca contents correspond to high proportions of crandallite $\text{CaAl}_3(\text{PO}_4)_2(\text{OH})_6$ (Figs.
349 8a,b,d);
- 350 iii. high As and high Ce contents correspond to high proportions of arsenoflorencite (Ce,
351 $\text{REE})\text{Al}_3(\text{AsO}_4)_2(\text{OH})_6$ (Figs. 8a,b).

352 APS minerals show wide compositional variations, but all can be expressed using the above five
353 end members (crandallite, goyazite, svanbergite, florencite, arsenoflorencite).

354 **Spatial, chemical and temporal variation of APS minerals and associated clay minerals**

355 Along the entire studied range of the P2 fault, APS minerals occur with sudoite (\pm illite,
356 magnesiofoitite) in metapelite and pegmatite. The APS minerals are florencitic, but contain
357 significant Ca, Sr, and SO_4^{2-} reflecting a minor component of svanbergite, mainly as core (Fig.
358 9).

359 Gaboreau et al. (2005, 2007) found that APS minerals proximal to uranium deposits
360 contain high LREE and P relative to those in intermediate and distal areas (Fig. 9). The present
361 study found a large compositional variation of APS minerals even within the ore compared to the
362 range presented by Gaboreau et al (2005, 2007) and compositional variation do not correlate with
363 distance from uranium mineralization (Fig. 9). For example, the $(\text{LREE}+\text{P})/(\text{Ca}+\text{Sr}+\text{S})$ ratios of
364 APS minerals near (<1 m) the uranium ore range from 1.6 to 5.6, whereas those from barren
365 samples far (>500 m) from mineralization vary from 2.8 - 4 (Fig. 9). We suggest that our data
366 reflects the evolution of fluids in the ore zone where the earlier fluids contained high in Ca, Sr
367 and SO_4^{2-} , and evolved to have high LREE and P. This proposed interpretation is supported by
368 compositional zoning of APS minerals with Ca, Sr and S -rich cores and LREE and P -rims (Fig.
369 5a).

370 APS minerals are abundant with kaolin and illite in one sample of the Bleached Zone
371 (MAC17) along the unconformity. These grains are Sr- and S-rich and similar in composition
372 within the sample but not with the APS minerals found along the P2 fault (Fig. 9). The average
373 composition of the APS minerals is
374 $\text{Ca}_{0.16}\text{Sr}_{0.68}\text{Ce}_{0.05}\text{La}_{0.03}\text{Nd}_{0.04}\text{Pr}_{0.01}(\text{Al}_{2.96}^{\text{III}}\text{Fe}_{0.02})(\text{PO}_3\text{O}_{0.94}\text{OH}_{0.06})_{1.50}(\text{SO}_4)_{0.54}(\text{AsO}_4)_{0.01}(\text{OH})_6$,

375 svanbergite_{0.54}-crandallite_{0.16}-goyazite_{0.14}-florencite_{0.13}. The data are comparable to APS mineral
376 compositions in distal sandstones by Gaboreau et al. (2007) (Fig. 9).

377 One Red-Green Zone sample of intensely altered metapelite (MAC412) footwall to the P2
378 fault, contain APS minerals with As- and Ce-rich cores and Ca, Sr, and S-rich rims together with
379 clinocllore and sudoite. The grains show similar Ca, Sr, and S contents with varying LREE and P
380 due to the presence of As that substitutes for P (Figs. 7a and 9). The average composition of these
381 grains is $(\text{Ca}_{0.31}\text{Sr}_{0.22}\text{Ce}_{0.32}\text{La}_{0.04}\text{Nd}_{0.02}\text{III}\text{Fe}_{0.15})(\text{Al}_{2.92}\text{III}\text{Fe}_{0.08})(\text{PO}_3\text{O}_{0.83}\text{OH}_{0.17})_{1.11}(\text{SO}_4)_{0.18}$
382 $(\text{AsO}_4)_{0.68}(\text{OH})_6$, arsenoflorencite(-Ce)_{0.39}-crandallite_{0.31}-svanbergite_{0.18}-goyazite_{0.12}. This is the
383 first documented occurrence of arsenoflorencite(-Ce) in Athabasca Basin.

384 APS minerals from the McArthur River deposit and the P2 fault show cores of
385 svanbergite-crandallite-goyazite rimmed by florencite (Figs. 4c-e,k,l, 5a). APS minerals from the
386 Red-Green Zone contain arsenoflorencite(-Ce) cores rimmed by svanbergite-crandallite-goyazite
387 (Figs. 4h, 5b, 8b). APS minerals of the Bleached Zone are svanbergite-crandallite-goyazite (Fig.
388 8). The zoning suggests the crystallization sequence of APS minerals in the study area. Early
389 crystallization of arsenoflorencite (Ce) was followed by svanbergite-crandallite-goyazite, and
390 finally florencite.

391 **Nature of fluids responsible for APS mineral formation**

392 APS minerals in the Bleached Zone sample contain high SO_4^{2-} contents, up to 0.59 apfu
393 (Figs. 7b,d, 8b-d), indicating relatively oxidizing conditions for their formation. These APS
394 minerals have close to svanbergite end-member composition (Fig. 10), with a minor goyazite and
395 crandallite component (Figs. 7b,d-f; 8a-d). The grains coexist with kaolin and illite (Fig. 4I),
396 which is the diagenetic assemblage in the Athabasca Group sandstones (Hoeve and Quit 1984;

397 Quirt 2001). Furthermore, the composition of the APS minerals is similar to those of diagenetic
398 origin reported in Athabasca and Kombolgie sandstones (Gaboreau et al. 2005, 2007), and other
399 sedimentary basins worldwide (Spötl, 1990; Gaboreau et al. 2005, 2007; Pe-Piper and Dolansky
400 2005; Gall and Donaldson 2006; Fig. 10). Therefore, the APS minerals of the Bleached Zone
401 along the unconformity most likely crystallized from an oxidizing, Ca-, Sr- and SO₄-rich,
402 diagenetic fluid of the overlying sandstones.

403 The oxidizing conditions of diagenetic fluids from sandstones are recorded as relict cores
404 of the APS minerals along the P2 fault in the basement (Figs. 4, 5a). These cores contain high Ca,
405 Sr and S and are similar in composition to diagenetic APS minerals in sandstones described
406 above. The S/P ratios of APS minerals as whole grains along the P2 fault are relatively low (<
407 0.16) compared to those of the Bleached Zone (0.36; Fig. 11). The lowest S/P ratios (< 0.06) are
408 found in areas of Zone 2 ore in the basement (Fig. 11b). The data shows that the SO₄²⁻ contents in
409 fluids decreased from the unconformity to the P2 fault and from non-mineralized areas along the
410 P2 fault to ore zone. This indicates the change from a relatively oxidized to a relatively reduced
411 environment. This modification of fluid chemistry may have taken place due to interaction of
412 fluids with graphite-rich basement rocks, as has been suggested by Gaboreau et al (2007).
413 Alternatively, it was caused by reduced fluids originated from the graphite-rich basement rocks
414 and supplied through faults. In either case, this redox change closer to the uranium ore is
415 consistent with the reduction of U⁶⁺ to U⁴⁺ necessary for the precipitation of uraninite. Therefore,
416 S/P ratios of APS minerals record the reduction of fluids associated with the uranium
417 mineralization

418 The spatial association of florencitic APS minerals with the McArthur River uranium
419 deposit (Fig. 2b) and their abundance within the deposit suggest the close relationship between

420 florencite and the uranium mineralization. This observation is consistent with that of Gaboreau
421 (2005, 2007). The APS minerals in metapelite and pegmatite along the entire 7 km of the P2 fault
422 studied are predominantly florencite with minor components of svanbergite-svanbergite-
423 crandallite-goyazite (Figs. 4d-e, 9). The alteration assemblage of sudoite, magnesiofoitite and
424 illite is also similar all along the P2 fault including the ore zone. The evidence suggests that
425 similar fluids passed along the entire P2 fault. These fluids were likely uranium-bearing because
426 APS minerals contain uranium (up to 16 ppm; Table 3).

427 The Red-Green Zone sample of metapelite (sample MAC412; Fig. 3d), 100 m laterally
428 away from the P2 fault contains As- and LREE-rich APS minerals (Figs. 7a,d, 8b; Table 2).
429 Arsenic in APS minerals occur as As^{5+} , replacing P^{5+} in the X-site of the crystal structure. These
430 As-bearing crystals show prominent zoning with cores of arsenoflorencite-(Ce) and rims of
431 crandillite-goyazite and svanbergite solid-solution (Figs. 5b, 7a,c; Table 2) with sharp
432 boundaries. The zoning suggests that arsenoflorencite-(Ce) formed earlier than the svanbergite-
433 goyazite of diagenetic origin. This arsenoflorencite-(Ce) may have formed in the very early stage
434 of diagenesis. If this is the case, As-rich APS minerals should be observed in sandstones.
435 However, there is no record of As-rich APS minerals in the Athabasca sandstone. Furthermore,
436 sharp boundaries between cores and with rims suggests that As-rich APS minerals formed before
437 the sandstone diagenesis. We suggest that, arsenoflorencite-(Ce) cores may have formed during
438 the paleo-weathering before the deposition of the Athabasca sandstones. This proposed
439 interpretation is further supported by the presence of As^{5+} in the APS minerals. Although As
440 contents are high in organic-rich shale (e.g., Ketris and Yudovich 2009), As is mostly fixed in
441 sulphide minerals (e.g., Ryan et al., 2013). For As to be incorporated in the APS minerals, it

442 must be oxidized to As^{5+} , which is stable in oxidizing, near-surface conditions (Smedley and
443 Kinniburgh 2002).

444 **APS minerals related to uranium deposits and role of P2 fault**

445 It has been suggested that APS minerals with florencitic compositions are
446 contemporaneous with uranium mineralization based on their occurrences within uranium
447 deposits (Quirt 1991; Gaboreau et al. 2005, 2007; Mercadier et al. 2011). Here we have shown
448 that APS minerals of florencitic composition are found along a 7 km strike length of the P2 fault,
449 even in areas barren of mineralization (Table 2; Fig. 9); although, as previously discussed, APS
450 minerals with the highest florencite component (reflecting relatively reducing conditions) are
451 found in proximity to ore (Figs. 9, 11). The APS minerals also contain elevated uranium contents
452 (Table 3; Fig. 6), suggesting that florencitic APS minerals crystallized from uranium-bearing
453 fluids that became reduced. The evidence supports that florencite was contemporaneous with
454 uranium mineralization.

455 Florencitic APS minerals are not found in the basement greater than ~50 m from the
456 centre of the P2 fault (Table 1; Fig. 9). The distribution of the APS minerals constrains the extent
457 of the fluid footprint, and suggests that the entire P2 fault was a conduit for an oxidizing
458 uranium-bearing fluid during mineralization. The P2 fault was also a site of redox change where
459 an initial oxidizing fluid became modified and relatively reducing.

460 **Implication**

461 APS minerals are very small in size, but ubiquitous in the altered metasedimentary rocks
462 along the P2 fault, which hosts the McArthur River uranium deposit. Previous researchers noted
463 the spatial association of florencitic APS minerals and uranium deposits and suggested their use

464 as an exploration vector (e.g., Gaboreau et al. 2007). Our study reveals that APS minerals record
465 the timing and characteristics of geological events, from paleoweathering, diagenesis to
466 uraniferous hydrothermal activity. We conclude that oxidizing diagenetic fluids travelled along
467 P2 fault and formed svanbergite-crandallite-goyazite. The fluid evolved to become reducing
468 through interaction with the basement rocks and formed florencite rims. Our study shows that
469 APS minerals are an excellent mineralogical tool to fingerprint fluid pathways. APS minerals
470 with similar chemistry (high florencite component) are found along a 7 km of strike length of the
471 P2 fault, including areas barren of uranium mineralization. This suggests that uranium-bearing
472 fluids likely passed along the entire P2 fault, but only produced uranium mineralization in
473 localized areas. This study confirms that APS minerals are good indicators in identifying
474 alteration related to uranium mineralization, thus they may be used, especially when having a
475 florencitic composition, to identify fertile structures associated with uranium deposits.

476 **Acknowledgments**

477 This project was funded by Natural Resources of Canada through Targeted Geoscience Initiative
478 Four (TGI-4) program; Research Affiliate Program Bursary to EEA and a grant to KH. We thank
479 Eric G. Potter, science leader for the TGI-4 uranium ore system project, at the Geological Survey
480 of Canada, for his continuous support. Cameco Corp provided their logistic support for our field
481 work at the McArthur River mine. Special thanks extend to Gerard Zaluski and Tom Kotzer, as
482 well as Aaron Brown, Doug Adams, Remi Labelle, and Brian McGill for their help and useful
483 suggestions. We also thank Glenn Poirier of the Museum of Nature for his help with SEM and
484 EMPA analysis, and Zhaoping Yang of the Geological Survey of Canada for her help during the
485 LA ICP-MS analysis. We also extend many thanks to the Associate Editor, Julien Mercadier, and
486 journal reviewers, David Quirt and unknown, of this manuscript.

487

References

- 488 Adlakha, E.E., Hattori, K., Zaluski, G., Kotzer, T., and Potter, E.G. (2014) Alteration within the
489 basement rocks associated with the P2 fault and the McArthur River uranium deposit,
490 Athabasca Basin. Geological Survey of Canada Open File 7462, 35 p, doi:10.4095/293364
- 491 Alexandre, P., Kyser, K., Polito, P., and Thomas, D. (2005) Alteration mineralogy and stable
492 isotope geochemistry of Paleoproterozoic basement-hosted unconformity-type uranium
493 deposits in the Athabasca Basin, Canada. *Economic Geology*, 100, 1547–1563.
- 494 Alexandre, P., Kyser, K., Jiricka, D., and Witt, G. (2012) Formation and evolution of the
495 Centennial unconformity-related uranium deposit in the South-Central Athabasca Basin,
496 Canada. *Economic Geology*, 107, 385 – 400.
- 497 Annesley, I. R., Madore, C., and Portella, P. (2005) Geology and thermotectonic evolution of the
498 western margin of the Trans-Hudson Orogen: evidence from the eastern sub-Athabasca
499 basement, Saskatchewan. *Canadian Journal of Earth Sciences*, 42(4), 573-597.
- 500 Beaufort, D., Patrier, P., Laverret, E., Bruneton, P., and Mondy, J. (2005) Clay alteration
501 associated with Proterozoic unconformity-type uranium deposits in the East Alligator
502 Rivers uranium field, Northern Territory, Australia. *Economic Geology*, 100(3), 515-536.
- 503 Bronkhorst, D., Mainville, A.G., Murdock, G.M., and Yesnik, L.D. (2012) McArthur River
504 Operation Northern Saskatchewan, Canada: National Instrument 43-101 Technical Report.
- 505 Cuney, M., Brouand, M., Cathelineau, M., Derome, D., Freiburger, R., Hecht, L., Kister, P.,
506 Lobaev, V., Lorilleux, G., Peiffert, C. and Bastoul, A.M. (2003) What parameters control
507 the high grade – large tonnage of the Proterozoic unconformity related uranium deposits?,
508 in Cuney, M., ed., *Uranium Geochemistry 2003*, International Conference, April 13-16
509 2003, Proceedings: Unité Mixte de Recherche CNRS 7566 G2R, Université Henri
510 Poincaré, Nancy, France, 123-126.

- 511 Derome, D., Cathelineau, M., Cuney, M., Fabre, C., Lhomme, T., and Banks, D. A. (2005)
512 Mixing of sodic and calcic brines and uranium deposition at McArthur River,
513 Saskatchewan, Canada: a Raman and laser-induced breakdown spectroscopic study of fluid
514 inclusions. *Economic Geology*, 100(8), 1529-1545.
- 515 Dill, H.G. (2001) The geology of aluminium phosphates and sulfates of the alunite group
516 minerals: a review. *Earth-Science Reviews*, 53(1), 35-93.
- 517 Gall, Q., and Donaldson, J.A. (2006) Diagenetic fluorapatite and aluminum phosphate sulfate in
518 the Paleoproterozoic Thelon Formation and Hornby Bay Group, northwestern Canadian
519 Shield. *Canadian Journal of Earth Sciences*, 43(5), 617-629.
- 520 Gaboreau, S., Beaufort, D., Vieillard, P., Patrier, P., and Bruneton, P. (2005) Aluminum
521 phosphate–sulfate minerals associated with Proterozoic unconformity-type uranium
522 deposits in the East Alligator River Uranium Field, Northern Territories, Australia. *The*
523 *Canadian Mineralogist*, 43(2), 813-827.
- 524 Gaboreau, S., Cuney, M., Quirt, D., Beaufort, D., Patrier, P., and Mathieu, R. (2007) Significance
525 of aluminum phosphate-sulfate minerals associated with U unconformity-type deposits:
526 The Athabasca Basin, Canada. *American Mineralogist*, 92(2-3), 267-280.
- 527 Hajnal, Z., White, D.J., Takacs, E., Gyorfi, I., Annesley, I.R., Wood, G., and Nimeck, G. (2010)
528 Application of modern 2-D and 3-D seismic-reflection techniques for uranium exploration
529 in the Athabasca Basin. *Canadian Journal of Earth Sciences*, 47(5), 761-782.
- 530 Hoeve, J., and Sibbald, T. I. (1978) On the genesis of Rabbit Lake and other unconformity-type
531 uranium deposits in northern Saskatchewan, Canada. *Economic Geology*, 73(8), 1450-
532 1473.

- 533 Hoeve, J., Rawsthorne, K., and Quirt, D. (1981) Uranium metallogenetic studies: Collins Bay B
534 Zone, II. Clay mineralogy. In: Summary of Investigations 1981, Saskatchewan Geological
535 Survey, Miscellaneous Report 81(4), 73-76.
- 536 Hoeve, J., and Quirt, D.H. (1984) Mineralization and host-rock alteration in relation to clay
537 mineral diagenesis and evolution of the Middle Proterozoic Athabasca Basin, Northern
538 Saskatchewan, Canada. Saskatchewan Research Council, Technical Report 189, 189 p.
- 539 Jambor, J. L. (1999) Nomenclature of the alunite supergroup. *The Canadian Mineralogist*, 37,
540 1323-1341.
- 541 Jefferson, C.W., Thomas, D.J., Gandhi, S.S., Ramaekers, P., Delaney, G., Brisbin, D., Cutts, C.,
542 Portella, P., and Olson, R. A. (2007) Unconformity-associated uranium deposits of the
543 Athabasca basin, Saskatchewan and Alberta; in EXTECH IV: Geology and Uranium
544 EXploration TECHnology of the Proterozoic Athabasca Basin, Saskatchewan and Alberta,
545 Geological Survey of Canada Bulletin, 588, 23-67.
- 546 Ketris, M.P., and Yudovich, Y.E. (2009) Estimations of Clarkes for carbonaceous biolithes:
547 World averages for trace element contents in black shales and coals. *International Journal*
548 *of Coal Geology*, 78(2), 135-148.
- 549 Laverret, E., Mas, P. P., Beaufort, D., Kister, P., Quirt, D., Bruneton, P., and Clauer, N. (2006)
550 Mineralogy and geochemistry of the host-rock alterations associated with the Shea Creek
551 unconformity-type uranium deposits (Athabasca Basin, Saskatchewan, Canada). Part 1.
552 Spatial variation of illite properties. *Clays and clay minerals*, 54(3), 275-294.
- 553 Lewry, J.F., and Sibbald, T. (1980) Thermotectonic evolution of the Churchill province in
554 northern Saskatchewan. *Tectonophysics*, 68, 45–82.

- 555 Longerich, H. P., Jackson, S. E., and Günther, D. (1996) Inter-laboratory note. Laser ablation
556 inductively coupled plasma mass spectrometric transient signal data acquisition and analyte
557 concentration calculation. *Journal of Analytical Atomic Spectrometry*, 11(9), 899-904.
- 558 Macdonald, C. (1985) Mineralogy and geochemistry of the sub-Athabasca regolith near
559 Wollaston Lake. *Geology of Uranium Deposits: Canadian Institute of Mining and
560 Metallurgy Special*, 32, 155-158.
- 561 McDonough, W.F., and Sun, S.S. (1995) The composition of the Earth. *Chemical Geology*,
562 120(3), 223-253.
- 563 McGill, B., Marlatt, J., Matthews, R., Sopuck, V., Homeniuk, L., and Hubregtse, J., (1993) The
564 P2 North uranium deposit, Saskatchewan, Canada. *Exploration and Mining Geology*, 2(4),
565 321- 333.
- 566 McKechnie, C. L., Annesley, I. R., and Ansdell, K. M. (2012) Medium-to low-pressure pelitic
567 gneisses of Fraser Lakes Zone B, Wollaston Domain, northern Saskatchewan, Canada:
568 mineral compositions, metamorphic P–T–t path, and implications for the genesis of
569 radioactive abyssal granitic pegmatites. *The Canadian Mineralogist*, 50(6), 1669-1694.
- 570 Mercadier, J., Cuney, M., Cathelineau, M., and Lacorde, M. (2011) U redox fronts and
571 kaolinisation in basement-hosted unconformity-related U ores of the Athabasca Basin
572 (Canada): late U remobilisation by meteoric fluids. *Mineralium Deposita*, 46(2), 105-135.
- 573 Mercadier, J., Richard, A., and Cathelineau, M. (2012). Boron- and magnesium-rich marine brines
574 at the origin of giant unconformity-related uranium deposits: $\delta^{11}\text{B}$ evidence from Mg-
575 tourmalines. *Geology*, 40(3), 231-234.
- 576 Morishita, T., Ishida, Y., Arai, S. (2005) Simultaneous determination of multiple trace element
577 compositions in thin (<30 μm) layers of BCR-2G by 193 nm ArF excimer laser ablation-

- 578 ICP-MS: implications for matrix effect and elemental fractionation on quantitative analysis.
579 *Geochemical Journal*, 39(4), 327-340.
- 580 Quirt, D., Kotzer, T., and Kyser, T.K. (1991) Tourmaline, phosphate minerals, zircon and
581 pitchblende in the Athabasca Group: Maw Zone and McArthur River areas. Saskatchewan.
582 Summary of Investigations 1991, Saskatchewan Geological Survey Miscellaneous Report
583 91-4, 11.
- 584 Quirt D.H. (2001) Kaolinite and dickite in the Athabasca Sandstone, Northern Saskatchewan,
585 Canada. Saskatchewan Research Council, Publication No. 10400-16D01.
- 586 Pe-Piper, G., and Dolansky, L.M. (2005) Early diagenetic origin of Al phosphate-sulfate minerals
587 (woodhouseite and crandallite series) in terrestrial sandstones, Nova Scotia, Canada.
588 *American Mineralogist*, 90(8-9), 1434-1441.
- 589 Ramaekers, P., Jefferson, C.W., Yeo, G.M., Collier, B., Long, D.G.F., Drever, G., McHardy, S.,
590 Jiricka, D., Cutts, C., Wheatley, K., Catuneau, O., Bernier, S., Kupsch, B., and Post, R.T.
591 (2007) Revised geological map and stratigraphy of the Athabasca Group, Saskatchewan
592 and Alberta; in EXTECH IV: Geology and Uranium EXploration TECHnology of the
593 Proterozoic Athabasca Basin, Saskatchewan and Alberta. Geological Survey of Canada
594 Bulletin, 588, 155-192.
- 595 Richard, A., Banks, D.A., Mercadier, J., Boiron, M.C., Cuney, M., and Cathelineau, M. (2011)
596 An evaporated seawater origin for the ore-forming brines in unconformity-related uranium
597 deposits (Athabasca Basin, Canada): Cl/Br and $\delta^{37}\text{Cl}$ analysis of fluid inclusions.
598 *Geochimica et Cosmochimica Acta*, 75(10), 2792-2810.
- 599 Riegler, T., Lescuyer, J.L., Wollenberg, P., Quirt, D., and Beaufort, D. (2014) Alteration related
600 to uranium deposits in the Kiggavik–Andrew Lake structural trend, Nunavut, Canada: New
601 insights from petrography and clay mineralogy. *The Canadian Mineralogist*, 52, 27- 45.

- 602 Ryan, P, Kim, J, Hattori, K., Thompson, A (2013) Dissolved arsenic in a fractured slate aquifer
603 system, northern Appalachians, USA: Influence of bedrock geochemistry, groundwater
604 flow paths, redox and ion exchange. *Applied Geochemistry*, 39, 181-192,
- 605 Spötl, C. (1990) Authigenic aluminium phosphate-sulfates in sandstones of the Mitterberg
606 Formation, Northern Calcareous Alps, Austria. *Sedimentology*, 37(5), 837-845.
- 607 Smedley, P.L., and Kinniburgh, D.G. (2002) A review of the source, behaviour and distribution
608 of arsenic in natural waters. *Applied Geochemistry*, 17(5), 517-568.
- 609 Stoffregen, R.E., Alpers, C.N., and Jambor, J.L. (2000) Alunite-jarosite crystallography,
610 thermodynamics, and geochronology. *Reviews in Mineralogy and Geochemistry*, 40(1),
611 453-479.

612 **Figure Captions**

613 **Figure 1.** A map showing the location of the major uranium deposits (red squares), including
614 McArthur River deposit, and basement structures (dashed lines), including the P2 fault, in the
615 Athabasca Basin (modified from Jefferson et al., 2007). The south-eastern margin of the
616 Athabasca Basin is underlain by the basement rocks of the Wollaston and Mudjatik Domains of
617 the western Churchill Province. An insert shows the locations of the Athabasca basin relative to
618 other two Mesoproterozoic sedimentary basins: Hornby and Thelon basins. Major shear zones:
619 BB = Black Bay, BLSZ= Black Lake Shear Zone, CB = Cable Bay, GR = Grease River Shear
620 Zone, RO = Robbilard, VRSZ = Virgin River Shear Zone.

621 **Figure 2.** Schematic cross-sections (**a, b**) showing the distribution of APS minerals, some sample
622 locations (stars) and a geologic map (**c**) at the unconformity showing sample locations. (**a**) APS
623 minerals are found in the P2 fault proximal to low-grade mineralization (sample MAC29) and in
624 the Bleached Zone (BZ) in quartzite (sample MAC17); (**b**) APS minerals are found in the P2

625 fault proximal to the Zone 2 ore body (samples MAC63, 67, 85, 152, 425). APS minerals were
626 not found in samples from the footwall and hanging-wall (indicated ``No APS``) nor in samples
627 collected from the VQ fault. (c) An interpreted geological strip map at the unconformity showing
628 the P2 fault, the locations of sampled drill-holes and ore bodies, sample locations, and the sites of
629 the cross sections AB. The P2 fault is essentially barren in the southwestern part. Low-grade
630 mineralization occurs along the middle and southeast (P2 Main deposit) portions of the P2 fault.
631 APS minerals were found in one sample (sample MAC412) of the Red-Green Zone in the
632 footwall proximal to the P2 Main mineralization. Z1 - 4 = Zone numbers of ore body at the
633 McArthur River deposit; uc = unconformity.

634 **Figure 3.** Photographs of selected drill-core samples; (a) uranium ore of the Zone 2 ore body and
635 P2 fault (MAC425); (b) intensely sudoite-altered pegmatite from the P2 fault (MAC67); (c)
636 quartzite from the Beached Zone along the unconformity (MAC17); and (d) hematitized and
637 chloritized metapelite from the Red-Green Zone (MAC412). Sample locations are shown in Fig.
638 2.

639 **Figure 4.** Photomicrographs (a, b, f) and SEM BSE (c-e, g-l) images of APS minerals. (a)
640 Disseminated APS grains in fine-grained illite (Ilt) and with hematite (Hem); (b) Clustered APS
641 grains in contact with an aggregate of feather-textured, magnesiofoitite (Mgf) and a mixture of
642 sudoite+illite+magnesiofoitite (Sud/Ilt/Mgf); (c) Zoned APS grains in magnesiofoitite; (d)
643 Oscillatory zoned APS crystals disseminated in a mixture of clinocllore+illite+magnesiofoitite
644 (Clc-Ilt-Mgf) with chalcopyrite (Ccp); (e) Zoned APS crystals clustered in
645 magnesiofoitite+sudoite; (f) Zoned APS crystals, apatite, and magnesiofoitite in a mixture of
646 sudoite+illite; (g) Partially corroded zircon (Zrn) mantled by xenotime (Xtm) and APS grains; (h)
647 Aggregate of euhedral, zoned APS crystals in a clinocllore+sudoite matrix; (i) Disseminated,

648 sub-hedral APS grains in fine-grained kaolin (Kln); **(j)** A mixture of APS minerals and quartz
649 rimming coarse quartz grain; **(k)** APS grain in contact with pyrite (Py); **(l)** APS crystal with
650 inclusions of Fe-oxide in contact with apatite (Ap). Sample number and location are indicated at
651 the bottom left corner of each image. Qz = Quartz

652 **Figure 5.** X-ray maps of APS minerals showing zoning with respect to Ca, Ce, Sr, S and P
653 obtained by wave-length dispersive spectra of EPMA: **(a)** sample MAC425 from the P2 fault and
654 Zone 2 ore body and **(b)** sample MAC412 from the Red-Green Zone (locations shown in Fig. 2a
655 and 2b; Table 2 for quantitative chemical data). svan-goy-crand = svanbergite-goyazite-
656 crandallite. Note that very dark areas in BSE images contain low mass elements and they are not
657 holes or other mineral inclusions.

658 **Figure 6.** Chondrite-normalized REE, U, Th, Pb and W for APS grains from sample MAC44
659 (along the P2 fault proximal to the Zone 3 ore body of the McArthur River deposit) and from
660 samples MAC63 and MAC85 (close to Zone 2 ore). The abundance of these elements was
661 obtained using EPMA (La, Ce, Pr and Nd) and LA-ICP-MS (Sm, Eu, Gd, Tb, Dy, Ho, Er, Tm,
662 Yb, Lu, W, Pb, Th and U). Error bars are not shown in the diagram because the uncertainty of the
663 analysis (< 10 %) is smaller than the size of symbols. Sample locations are in Figure 2c and
664 Table 1. Each line represents one APS grain. Chondrite values from McDonough and Sun (1995).

665 **Figure 7.** Binary plots showing substitution and elemental relationships of APS minerals based
666 on EPMA data: **(a)** As vs P (black) and As vs. Ce (gray); **(b)** S vs. Sr (black) and S vs. Ce (gray);
667 **(c)** P vs Sr (black) and P vs. LREE (gray); **(d)** S vs. As (black) and S vs. P (gray); and **(e)** LREE
668 vs. Sr (black) and LREE vs. Ca (gray). Each data point represents one grain. P2 fault = P2 fault
669 samples (triangles). BZ = Bleached Zone sample (stars), RGZ = Red-Green Zone sample
670 (crosses).

671 **Figure 8.** Compositions of APS minerals plotted on ternary diagrams. End member minerals are
672 indicated at the apexes of the diagrams. **(a)** Ca-Sr-LREE; **(b)** P-S-As; **(c)** S-Sr-LREE; **(d)** S-Sr-
673 Ca. Each data point represents one grain. P2 fault = P2 fault samples (triangles). BZ = Bleached
674 Zone sample (stars), RGZ = Red-Green Zone sample (crosses).

675 **Figure 9.** Cross-plot showing coupled substitution of Ca-Sr-S for LREE-P for APS minerals
676 along the P2 fault (triangles), and within the Bleached Zone (BZ) sample (stars) and Red-Green
677 Zone (RGZ) (crosses). P2 fault samples are color coded with respect to distance in metre from the
678 uranium mineralization (McArthur River deposit and low-grade): red filled triangles represents
679 sample < 1 m from ore (MAC425 and MAC29), orange filled triangles were < 15 m from ore
680 (MAC152), purple filled triangles were < 20 m from ore (MAC67 and MAC85), open green
681 triangles were < 50 m from ore (MAC43, MAC44, MAC63 and MAC404) and open blue
682 triangles were of unmineralized areas >500 m from the ore (MAC117 and MAC135). Each data
683 point represents one grain. For comparison, the diagram shows the compositional ranges of APS
684 minerals determined by Gaboreau et al (2005, 2007) from the Athabasca Basin (fields with
685 various shades of gray) and Kombolgie Basin, Australia (field with various shades of blue).

686 **Figure 10.** An alunite-goyazite-crandallite [S-Sr-Ca] ternary plot showing compositions of APS
687 minerals from the P2 fault (P2; triangles), the Bleached Zone (BZ; stars) sample, and the Red-
688 Green Zone (RGZ; crosses) sample. Each data point represents one grain. For comparison, the
689 compositional ranges of diagenetic APS minerals from various sedimentary units are shown:
690 diagenetic APS minerals of the Athabasca and Kombolgie basins are represented by grey dotted
691 field (Gaboreau et al. 2005, 2007) and diagenetic APS minerals of the Chaswood Formation (Pe-
692 Piper and Dolansky, 2005), Hornby Basin and Thelon Basins (Gall and Donaldson, 2006) and
693 Mitterberg Formation (Spötl, 1990) are collectively represented by the grey field. APS minerals

694 associated with uranium deposits of the Athabasca and Komolgie Basin (Gaboreau et al. 2005,
695 2007) are represented by the black dashed field.

696 **Figure 11:** Spatial variation of S/P ratios for APS minerals. The average S/P ratio (mixed data,
697 see Table 2) of APS minerals within a sample is expressed as a red, bold, italicized number next
698 to its corresponding sample ((a) and (b)) or drill-core (c) location.

699

Appendix

700 **Figure 1:** (a) A graph of the LA-ICP-MS analysis of an APS grain from sample MAC85
701 showing element counts (major and trace) vs. time in seconds. High counts of Y, Th and U
702 correlate with high counts of the major elements in APS minerals (eg., Ce, La, Al, and Sr). This
703 graph clearly shows that trace elements (such as Y, Th and U) are incorporated in the APS crystal
704 structure and were not present as inclusions or contributed by surrounding minerals of sudoite
705 (Sud) or illite (Ilt). (b) The same graph as shown in (a) but counts/sec of each element is
706 normalized to that of Sr.

707 **Figure 2:** An APS mineral (a) before EMPA analysis and (b) after analysis showing beam
708 damage. (c) A laser pit after LA ICP-MS analysis. (a) and (c) are BSE images and (b) is a
709 secondary electron image.

710 **Figure 3:** A binary plot comparing the average concentrations of Ca (green), Fe (red), Pr (cyan)
711 and Nd (blue) in APS mineral grains from samples MAC44 (diamonds), MAC63 (x), and
712 MAC85 (crosses) obtained with EMPA (Table 2) and LA ICP-MS (Table 3). Horizontal and
713 vertical bars represent one standard deviation of the data (Tables 2 and 3). LA ICP-MS data of
714 sample MAC85 is of one grain.

Table 1: Sample descriptions.

zone ^a	DDH ^b	sample	depth ^c	proximity to P2 fault ^d	proximity to uc ^d	proximity to U-min ^d
P2	MC370	MAC29	560.2	in the P2 fault zone	u/c (Fig. 2A)	<1 m from lg U-min in ss
	H729	MAC43	49.5	in the P2 fault zone	~15 m	<50 m from Z3 ore
	H729	MAC44	64.5	~15 m laterally from P2 in fw	~15 m	<50 m from Z3 ore
	H201	MAC63	7.6	~30 m laterally from P2 in hw	~20 m	<50 m from Z2 ore
	H201	MAC67	30.8	the P2 fault zone	~20 m	<20 m from Z2 ore
	H493	MAC85	17.7	in the P2 fault zone	~20 m	<20 m from Z2 ore
	H203	MAC152	62	in the P2 fault zone	~50 m	<15 m from Z2 ore
	MC410	MAC404	542.7	~50 m laterally from P2 in hw	~15 m	~50m laterally from lg in ss
	H3380	MAC425	57.1	in the P2 fault zone	~50 m	Z2 ore
	MC361	MAC117	523.3	in the P2 fault zone	~25 m	>500 m from U-min
	MC362	MAC135	520.2	~40 m above P2 in hw	~10 m	>500 m from U-min
GRZ	MC346	MAC412	669	~100 m laterally from P2	~50 m	~100 m below P2 Main
BZ	MC344	MAC17	499.4	~250 m laterally from P2 in hw	<1 m	>250 m from U-min

Notes:

^aP2 = P2 fault sample; RGZ = Red-Green Zone sample; BZ = Bleached Zone sample

^bDDH= diamond drill-hole number

^cdrillhole with the prefix H are collared underground, therefore sample depths are not from the surface

^dU-min= uranium mineralization in the McArthur River deposit; fw= footwall; hw = hangingwall; lg = low-grade (<1 wt% U₃O₈); ss

^eAp = apatite; Clc = clinocllore; Dck = dickite; Drv = dravite; Fe-Mg chl = Fe-Mg Chlorite; fg = fine-grained; Gr = graphite; Illt = illi

degree of alteration and rock-type ^d	APS occurrence	clay ^e	mineralogy ^f
moderately altered mp	isolated, 3-10 μm	Sud	Mgf, Xtm, Qz
green intensely altered graphitic mp	isolated, 3-10 μm	Sud/Ilt	Mgf, Gr, Py, Ap, Zrn, Xtm
red and white intensely altered peg	zoned, clustered, 5-20 μm	Sud/Ilt	Hem, Mnz, Zrn, Qz, Gr, Py
green intensely altered mp	zoned, clustered, fragmented, 1-20 μm	Sud	Ilt, Rt, Ap, Fe-Mg Chl, Ilt, Py, Qz
green intensely altered peg	zoned, clustered, 5-20 μm	Sud	Mgf, Ilt, Py, Ap, Qz
intensely altered graphitic mp w/ peg boudins	zoned, disseminated, 5-20 μm	Sud/Ilt	Drv, Py
green-white intensely altered mp	zoned, disseminated, 5-30 μm	Sud/Clc	Mgf, Ill, Py, Qz, Ccp
red moderately altered mp w/ peg boudins	disseminated, < 1 μm	Kln	Hem, Ap
green intensely altered mp with U-ore	some cores missing, isolated, 3-10 μm	Mgf/Sud	U, Hem
white-green intensely altered peg	isolated, 3-10 μm	Ilt	Fe-Mg Chl, fg Qz, Qtz
red-green intensely altered peg	disseminated, < 1 μm	Ilt	Hem, Rt, fg Qz
red-green intensely altered mp	large clusters up to .5 mm, 10-40 μm	Sud/Clc	Hem
quartzite with bleached matrix	disseminated, < 1 μm	Kln	Ilt, Zrn, Qz

= sandstone; uc = unconformity; peg = pegmatite; mp = metapelite

ite; Mgf = magnesiofoidite, Py = pyrite; Qz = quartz; Rt = rutile sud = sudoite, U = uraninite; xtm = xenotime; zrn = zircon

Table 2: EMPA major element oxide data and atomic proportion formula units for APS minerals.

sample	MAC67		MAC85		MAC152		MAC404		MAC117		MAC425		MAC
	Sud	Mixed	Sud/Ilt	Mixed	Sud/Clc	Core	Rim	KIn	Ilt	Mixed	Mgf/Sud	Mixed	Ilt
a													
# grains	10 1σ	8 1σ	11 1σ	3 1σ	3 1σ	3 1σ	3 1σ	10 1σ	10 1σ	10 1σ	9 1σ	9 1σ	3
CaO	2.72 0.30	2.86 0.44	2.70 0.36	2.92 0.24	2.92 0.24	2.37 0.31	2.37 0.31	3.40 0.18	2.68 0.36	2.68 0.36	2.79 0.67	2.79 0.67	3.14
SO ₃	1.68 0.77	2.06 0.53	1.69 1.29	2.58 0.44	2.58 0.44	1.14 0.30	1.14 0.30	0.94 0.37	3.70 0.46	3.70 0.46	3.43 1.48	3.43 1.48	3.40
Al ₂ O ₃	28.96 1.56	32.01 1.08	31.26 1.30	32.30 0.31	32.30 0.31	31.26 0.63	31.26 0.63	31.13 1.25	32.22 1.07	32.22 1.07	32.37 1.10	32.37 1.10	29.49
Fe ₂ O ₃	0.85 0.77	0.54 0.24	0.54 0.51	0.58 0.24	0.58 0.24	0.44 0.05	0.44 0.05	0.91 0.63	0.82 0.71	0.82 0.71	0.96 0.57	0.96 0.57	1.40
Nd ₂ O ₃	3.26 0.44	2.77 0.50	3.29 0.79	2.44 0.33	2.44 0.33	3.80 0.47	3.80 0.47	4.26 0.37	2.16 0.42	2.16 0.42	2.20 0.36	2.20 0.36	1.41
Pr ₂ O ₃	0.94 0.16	0.76 0.21	0.87 0.23	0.75 0.08	0.75 0.08	0.97 0.08	0.97 0.08	0.96 0.06	0.60 0.12	0.60 0.12	0.70 0.15	0.70 0.15	0.50
Ce ₂ O ₃	8.67 1.21	7.81 0.78	8.33 1.09	7.74 0.37	7.74 0.37	9.44 0.54	9.44 0.54	7.50 0.48	7.85 0.80	7.85 0.80	7.50 1.78	7.50 1.78	8.81
La ₂ O ₃	5.40 0.82	5.18 0.47	5.55 0.31	5.11 0.29	5.11 0.29	5.33 0.42	5.33 0.42	3.58 0.19	5.58 0.87	5.58 0.87	4.50 1.22	4.50 1.22	2.83
P ₂ O ₅	25.84 1.71	27.10 0.58	26.76 1.17	26.66 0.64	26.66 0.64	28.20 0.27	28.20 0.27	28.85 1.43	25.24 0.73	25.24 0.73	25.71 1.17	25.71 1.17	26.65
SiO	3.14 0.64	3.73 0.62	3.17 1.08	4.09 0.37	4.09 0.37	2.64 0.25	2.64 0.25	3.65 0.74	4.38 0.45	4.38 0.45	5.49 1.64	5.49 1.64	5.95
ThO ₂	0.51 0.29	0.16 0.05	0.27 0.38	0.15 0.09	0.15 0.09	0.11 0.07	0.11 0.07	0.15 0.10	0.04 0.02	0.04 0.02	0.13 0.09	0.13 0.09	0.27
As ₂ O ₅	0.02 0.01	0.01 0.01	0.02 0.02	0.01 0.01	0.01 0.01	0.01 0.01	0.01 0.01	0.06 0.05	0.04 0.01	0.04 0.01	0.01 0.02	0.01 0.02	0.13
Total	81.98 2.61	84.98 0.92	84.46 1.99	85.34 0.96	85.34 0.96	85.70 0.76	85.70 0.76	85.40 0.89	0.04 1.40	0.04 1.40	85.78 1.45	85.78 1.45	83.97
SiO ₂ ^c	1.44 1.54	0.39 0.10	0.63 0.30	0.41 0.12	0.41 0.12	0.36 0.29	0.36 0.29	5.85 4.21	1.19 0.77	1.19 0.77	1.88 1.44	1.88 1.44	6.75
apfu													
Ca	0.25	0.25	0.24	0.25	0.25	0.21	0.21	0.29	0.23	0.23	0.24	0.24	0.28
Sr	0.16	0.17	0.16	0.19	0.19	0.13	0.13	0.17	0.21	0.21	0.25	0.25	0.28
Nd	0.10	0.08	0.10	0.07	0.07	0.11	0.11	0.12	0.06	0.06	0.06	0.06	0.04
Pr	0.03	0.02	0.03	0.02	0.02	0.03	0.03	0.03	0.02	0.02	0.02	0.02	0.02
Ce	0.27	0.23	0.25	0.23	0.23	0.28	0.28	0.22	0.23	0.23	0.22	0.22	0.27
La	0.17	0.16	0.17	0.15	0.15	0.16	0.16	0.11	0.17	0.17	0.13	0.13	0.09
Fe ³⁺		0.03	0.03	0.04	0.04	0.03	0.03	0.02	0.05	0.05	0.06	0.06	
Al		0.06	0.05	0.07	0.07	0.02	0.02		0.07	0.07			
Th	0.01												0.01

A	1.00	1.02	1.00	1.02	0.97	1.04	0.99	0.97
Al	2.95	3.00	3.00	3.00	2.96	3.00	3.06	2.86
Fe ³⁺	0.06				0.04	0.00	0.00	0.09
B	3.01	3.00	3.00	3.00	3.00	3.00	3.06	2.95
P	1.89	1.87	1.86	1.82	1.97	1.73	1.75	1.86
S	0.11	0.10	0.12	0.16	0.06	0.23	0.21	0.21
As								0.01
X	2.00	1.97	1.98	1.98	2.03	1.96	1.95	2.07
ΣLREE	0.58	0.54	0.51	0.47	0.58	0.48	0.44	0.41
Ce anomaly ^d	0.83	0.81	0.85	0.85	0.89	0.92	0.90	1.59
S/P	0.06	0.05	0.06	0.09	0.04	0.13	0.12	0.11

Notes:

Due to small grain size of APS minerals and the relatively large electron beam size (5 μm) for the analysis, it was difficult to obtain precise composition of individual compositional zones in grains, as some rims are narrower than 5 μm. Most cores are also smaller than 5 μm (Figs. 4,5). Therefore, most of the compositional data presented in Table 2 reflect mixtures of different zones. Rim and core analysis was conducted on two samples containing relatively large APS (MAC152 and MAC412).

a: adjacent minerals, Illt=illite, Sud=sudoite, Mgf = magnesiofotite; Clc = clinocllore

b: Area of analysis in grains, ie. rim, core or mixed. Compositional zones are narrower than the beam size of 5 μm. The mixed area

refers to the data from different compositional zones defined in SEM-BSE images

c: contribution of surrounding minerals in the analytical data was evaluating using SiO2 contents (see the Results for detailed description)

d: $[Ce]_N^* = \sqrt{([La]_N \cdot [Pr]_N)}$

135	GRZ										BZ					
	MAC63		MAC29		MAC44		MAC43		MAC412			MAC17				
	Sud Mixed	7 1σ 3.34 0.31 4.49 0.35 32.82 0.64	Sud Mixed	4 1σ 1.95 0.26 3.14 0.83 30.28 1.90	Sud/Ilt Mixed	14 1σ 3.18 0.19 4.80 0.71 32.52 0.78	Sud/Ilt Mixed	2 1σ 2.98 0.45 5.86 1.33 31.99 0.46	Mixed	10 1σ 3.49 0.36 2.84 0.24 30.15 1.01			Sud/Clc Core	2 1σ 3.46 0.42 2.89 0.17 28.78 0.65	Rim	2 1σ 3.87 0.44 3.27 0.53 31.57 1.76
0.56	0.23 0.11	1.90 0.87	0.50 0.19	0.31 0.14	3.49 1.66	5.85 2.02	3.37 2.99	0.34 0.11	3.49 1.66	5.85 2.02	3.37 2.99	0.34 0.11	3.49 1.66	5.85 2.02	3.37 2.99	0.34 0.11
0.17	2.79 0.54	2.62 0.33	1.84 0.19	2.26 0.37	0.68 0.26	0.74 0.02	0.48 0.23	1.21 0.32	0.68 0.26	0.74 0.02	0.48 0.23	1.21 0.32	0.68 0.26	0.74 0.02	0.48 0.23	1.21 0.32
0.12	0.71 0.16	0.76 0.09	0.58 0.12	0.46 0.17	0.12 0.09	0.25 0.08	0.19 0.07	0.31 0.25	0.12 0.09	0.25 0.08	0.19 0.07	0.31 0.25	0.12 0.09	0.25 0.08	0.19 0.07	0.31 0.25
0.63	6.75 0.46	4.65 0.70	6.07 0.70	5.84 0.44	11.16 0.80	9.40 1.05	10.19 1.26	1.71 0.64	11.16 0.80	9.40 1.05	10.19 1.26	1.71 0.64	11.16 0.80	9.40 1.05	10.19 1.26	1.71 0.64
0.27	3.78 1.01	4.08 1.33	3.95 0.47	3.28 0.25	1.32 0.39	1.56 0.52	1.26 0.74	1.01 0.36	1.32 0.39	1.56 0.52	1.26 0.74	1.01 0.36	1.32 0.39	1.56 0.52	1.26 0.74	1.01 0.36
0.66	25.52 0.63	23.95 0.49	25.61 0.73	25.09 0.85	15.56 2.78	13.02 0.36	21.64 3.87	20.66 0.97	15.56 2.78	13.02 0.36	21.64 3.87	20.66 0.97	15.56 2.78	13.02 0.36	21.64 3.87	20.66 0.97
0.74	5.01 0.61	6.27 0.68	6.77 0.79	7.01 1.59	4.52 0.58	4.51 0.23	5.18 1.69	13.70 0.74	4.52 0.58	4.51 0.23	5.18 1.69	13.70 0.74	4.52 0.58	4.51 0.23	5.18 1.69	13.70 0.74
0.06	0.08 0.05	0.19 0.09	0.02 0.03	0.04 0.01	0.01 0.01	0.02 0.02	0.01 0.01	0.06 0.03	0.01 0.01	0.02 0.02	0.01 0.01	0.06 0.03	0.01 0.01	0.02 0.02	0.01 0.01	0.06 0.03
0.05	0.02 0.02	0.05 0.03	0.01 0.01	0.05 0.03	15.72 4.32	17.85 0.79	6.04 5.16	0.24 0.06	15.72 4.32	17.85 0.79	6.04 5.16	0.24 0.06	15.72 4.32	17.85 0.79	6.04 5.16	0.24 0.06
1.17	85.56 1.25	79.85 1.57	85.86 1.46	85.19 0.74	89.04 1.16	88.34 0.22	87.07 0.96	78.75 1.90	89.04 1.16	88.34 0.22	87.07 0.96	78.75 1.90	89.04 1.16	88.34 0.22	87.07 0.96	78.75 1.90
1.47	0.84 0.35	8.32 3.91	0.88 0.30	0.98 0.17	0.70 0.59	0.70 0.22	0.69 0.58	9.74 5.57	0.70 0.59	0.70 0.22	0.69 0.58	9.74 5.57	0.70 0.59	0.70 0.22	0.69 0.58	9.74 5.57
	0.28	0.18	0.27	0.25	0.31	0.31	0.33	0.16	0.31	0.31	0.33	0.16	0.31	0.31	0.33	0.16
	0.23	0.31	0.31	0.32	0.18	0.22	0.24	0.68	0.18	0.22	0.24	0.68	0.18	0.22	0.24	0.68
	0.08	0.08	0.05	0.06	0.02	0.02	0.01	0.04	0.02	0.02	0.01	0.04	0.02	0.02	0.01	0.04
	0.02	0.02	0.02	0.01	0.02	0.02	0.01	0.01	0.02	0.02	0.01	0.01	0.02	0.02	0.01	0.01
	0.20	0.15	0.18	0.17	0.34	0.29	0.30	0.05	0.34	0.29	0.30	0.05	0.34	0.29	0.30	0.05
	0.11	0.13	0.12	0.10	0.04	0.05	0.04	0.03	0.04	0.05	0.04	0.03	0.04	0.05	0.04	0.03
	0.01	0.12	0.03	0.02	0.14	0.21	0.17		0.14	0.21	0.17		0.14	0.21	0.17	
	0.08		0.03	0.01												

1.01	0.99	1.00	0.95	1.03	1.10	1.09	0.98
3.00	3.06	3.00	3.00	2.92	2.84	2.96	2.96
0.00	0.00	0.00	0.00	0.08	0.16	0.04	0.02
3.00	3.06	3.00	3.00	3.08	3.00	3.00	2.98
1.72	1.74	1.71	1.70	1.08	0.92	1.46	1.50
0.27	0.20	0.28	0.35	0.18	0.18	0.19	0.54
1.99	1.94	2.00	2.05	1.89	1.88	1.91	2.05
0.41	0.38	0.36	0.35	0.63	0.78	0.26	0.01
0.89	0.57	0.86	1.02	6.00	3.25	4.42	0.65
0.16	0.12	0.17	0.21	0.17	0.20	0.13	0.36

Table 3: LA-ICPMS data of APS (ppm).

Sample: # grains	44 3 1 σ	63 3 1 σ	85 1	BCR2G ^a 1 σ	precision %	accuracy ^b %
Li	150 19	190 16	150	9 0.97	1.3	0.78
Si	48000 12000	68000 12000	99000	247000 3900	1.11	2.5
Ca	15000 1000	13000 3000	18000	48000 540	1.2	6.8
Sc	8.1 1.7	4.9 0.80	<3	28 0.35	0.46	14
Ti	31 17	26 5.5	52	12000 83	1.13	13
V	20 10	20 7.5	13	400 1.43	1.08	4.7
Cr	31 12	16 3.6	<30	15 0.29	0.50	18
Mn	30 7.6	18 5.8	55	1560 2.11	0.27	2.9
Fe	7600 1600	6300 3100	3500	85000 1300	1.48	12
Co	4.0 0.42	70 96	3.7	36 0.05	0.46	2.4
Ni	21.43 1.21	49 43	<10	10 0.82	1.07	
Cu	5.4 0.53	5.7 0.79	72	16 0.12	0.67	16
Zn	4.4 0.19	9.0 4.7	<8	150 1.4	1.56	15
Se	130 2.6	120 20	130	<3	1.85	
Rb	17 11	2.0 0.23	5.0	46 0.45	0.40	4.9
Sr	42000 7000	23000 6300	24000	310 2.7	0.79	10
Y	57 7.6	38 2.7	60	28 0.025	1.16	23
Zr	1.1 0.66	7.0 2.1	7.1	160 0.87	0.35	17
Nb	0.28 0.16	0.15 0.04	<0.3	10 0.01	0.53	
Mo	3.4 1.3	8.3 9.5	<4	240 0.86	1.06	3.1
Sn	2.3 0.86	3.3 1.2	2	2 0.03	1.08	
Ba	630 63	250 74	440	620 9.6	0.72	9.9
La	20000 3500	24000 5300	34200	23 0.25	1.36	6.3
Ce	39000 8000	45000 9400	58000	50 0.97	0.70	11
Pr	3800 500	4600 840	5900	5.8 0.035	0.75	15
Nd	14000 1400	17000 3200	20400	26.0 0.74	1.21	7.3
Sm	2000 69	2200 440	2800	5.7 0.17	0.68	14
Eu	760 87	800 200	1300	1.8 0.059	0.67	9.0
Gd	820 68	450 69	810	6.0 0.42	1.05	11
Tb	43 7.6	17 1.5	40	0.9 0.012	1.28	15

Dy	64	10	28.63	2.3	60	6	0.01	0.99	10
Ho	3.8	0.94	2.3	0.29	3.7	1.2	0.0095	0.84	10
Er	2.9	1.9	2.8	0.58	4	3	0.095	1.24	28
Tm	0.25	0.11	0.148	0.017	0.27	0.40	0.02	1.37	18
Yb	0.94	0.34	1.4	0.45	1.7	2.8	0.21	0.77	20
Lu	0.13	0.033	0.14	0.081		0.41	0.032	0.75	11
Hf	0.91	0.40	0.30	0.099	<0.53	4.3	0.23	1.32	11
Ta	0.17	0.10	0.077	0.08	<0.161	0.6	0.007	1.56	
W	0.79	0.36	0.9	0.029	1	0.5	0.03	0.61	
Pb	160	10	120	39	260	10.3	0.005	0.92	12
Th	1300	200	1100	140	2300	5.4	0.035	0.91	13
U	0.62	0.19	2.4	1.1	16	1.7	0.065	1.46	1.9

^aBCR2G from US Geological Survey

^bbased on the data of BCR2G provided by USGS

data is the average of analyzed grains (# grains) in the sample (± 1 standard deviation)

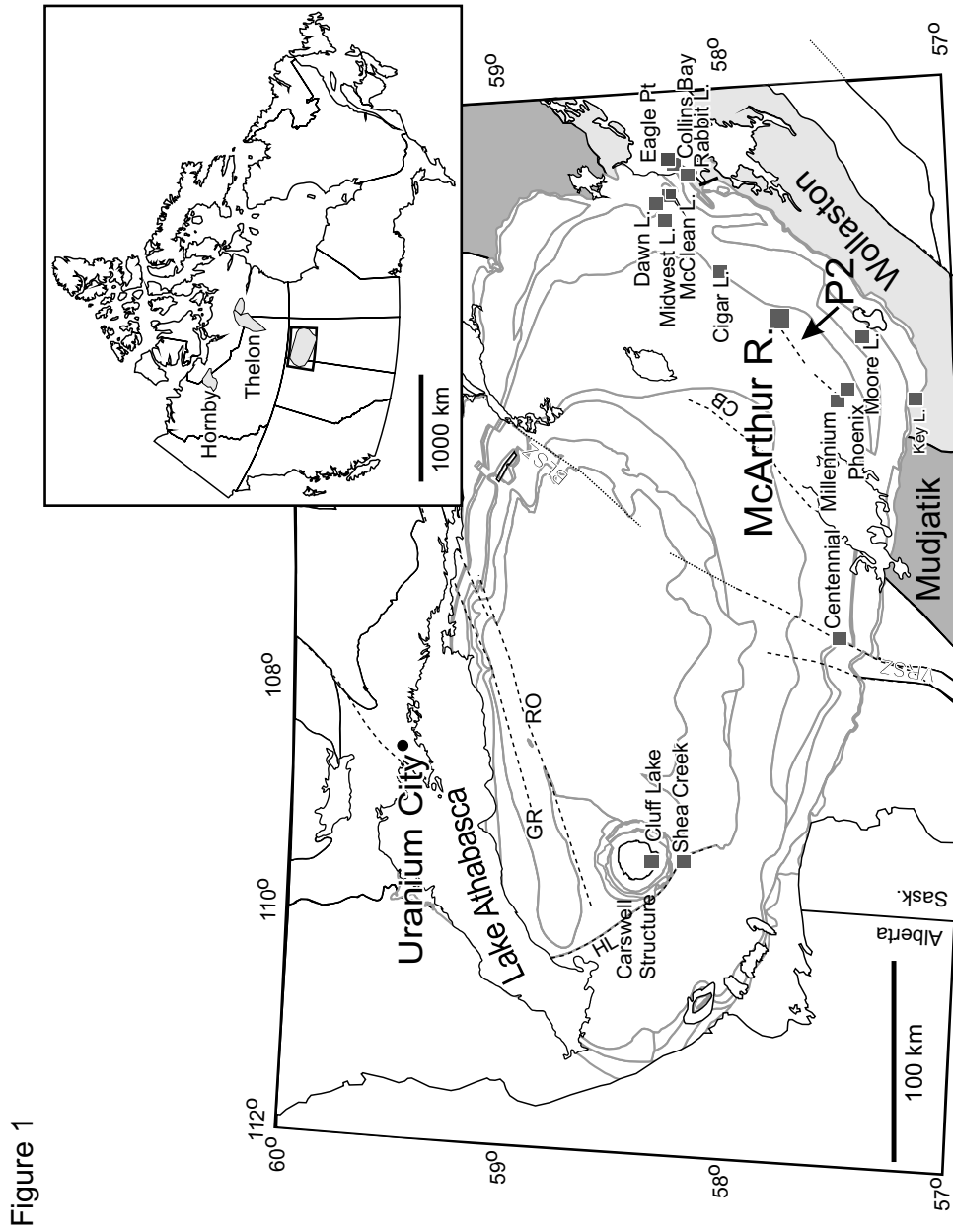


Figure 1

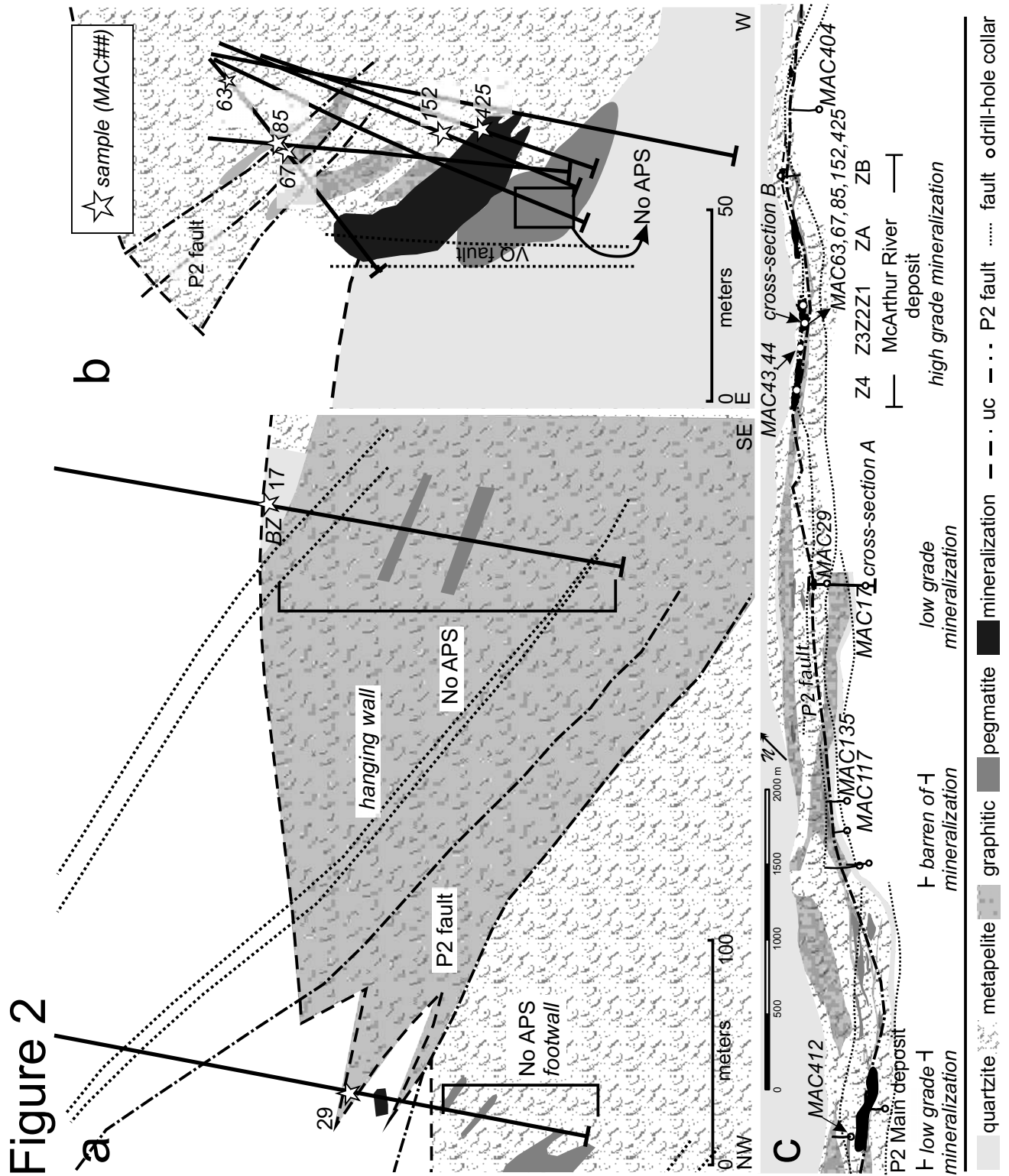


Figure 3



Figure 4

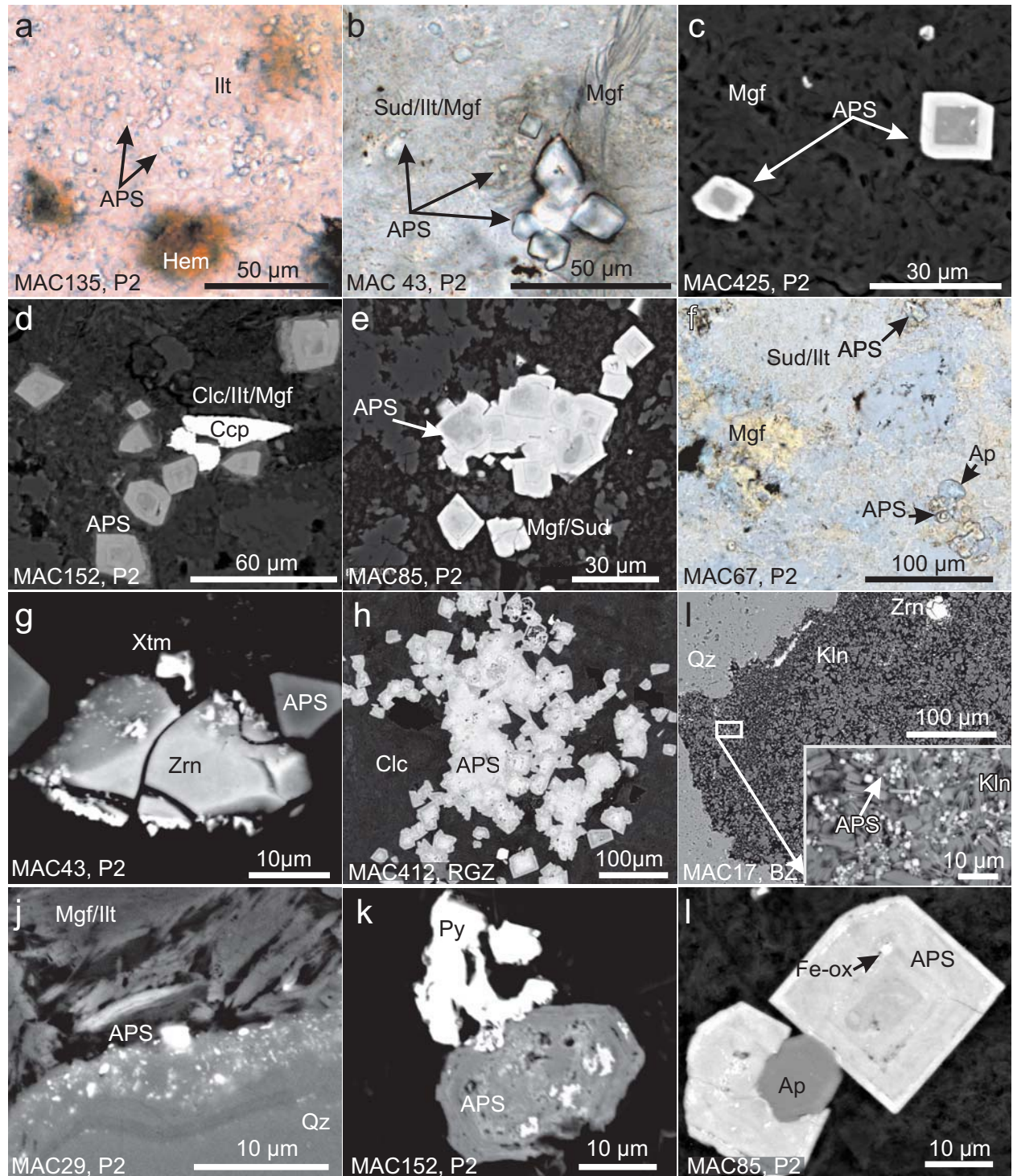
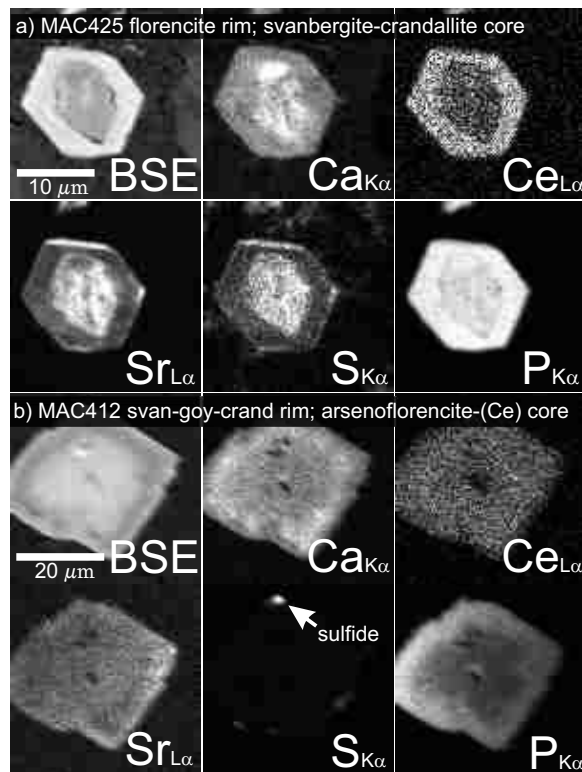


Figure 5



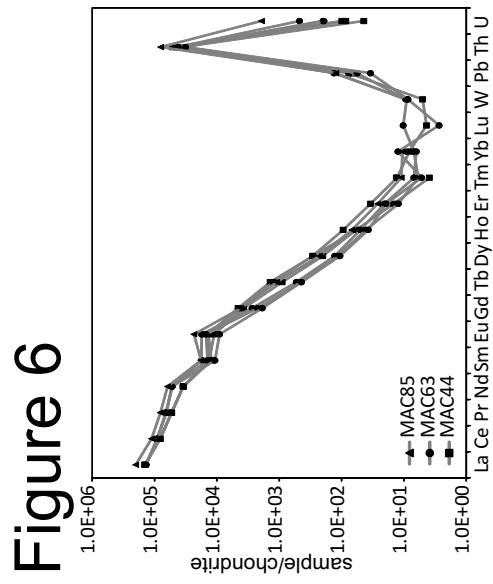
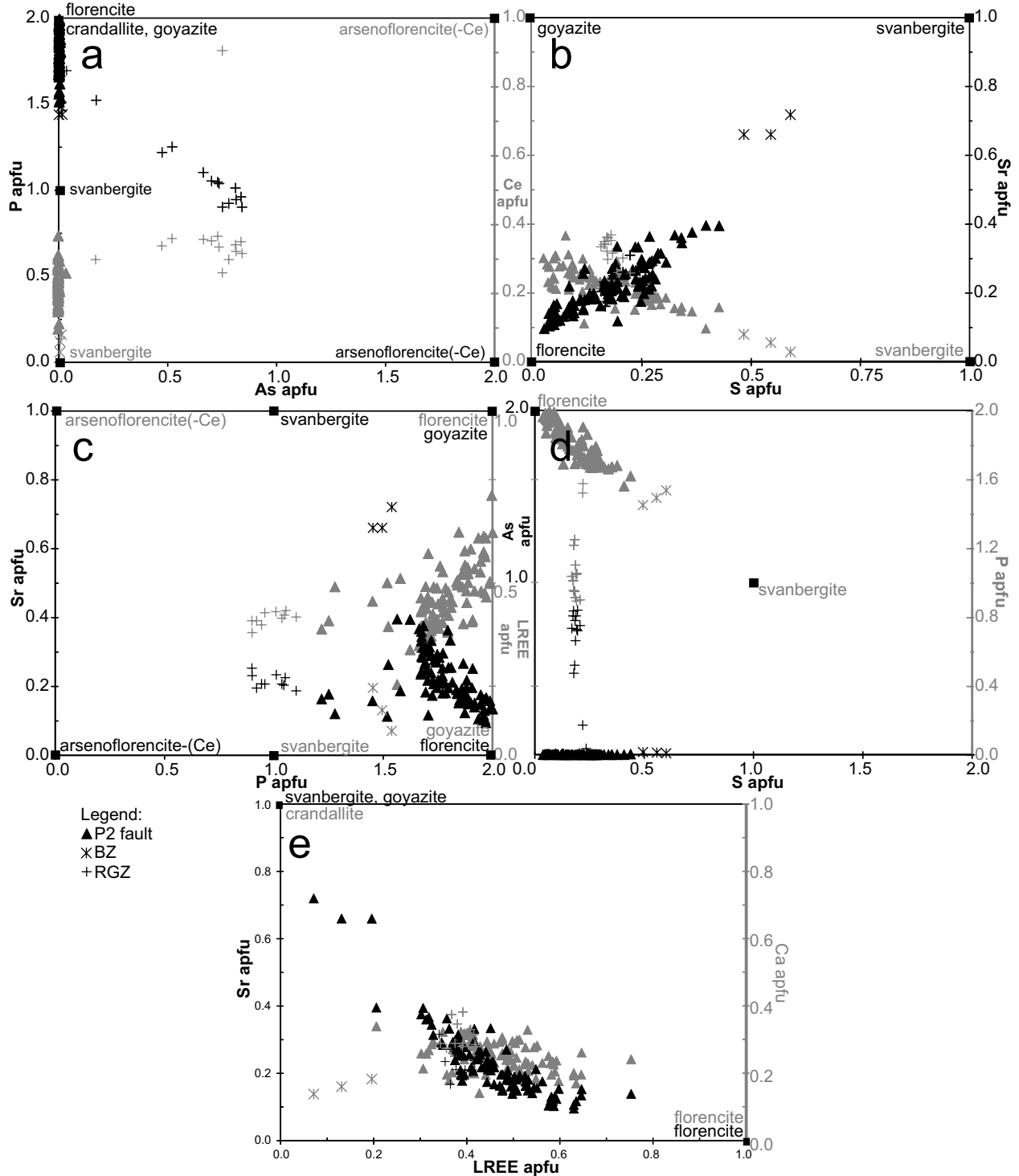


Figure 7



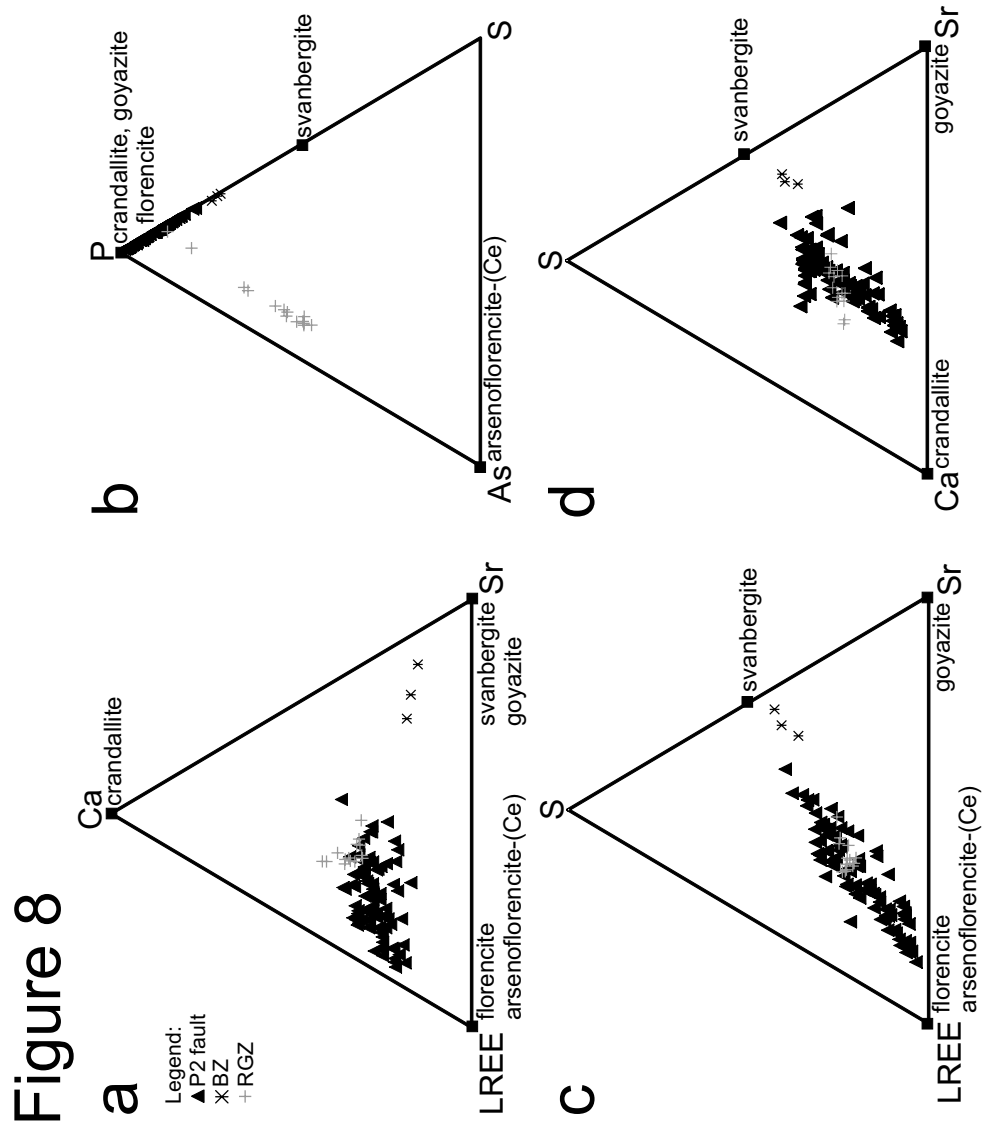
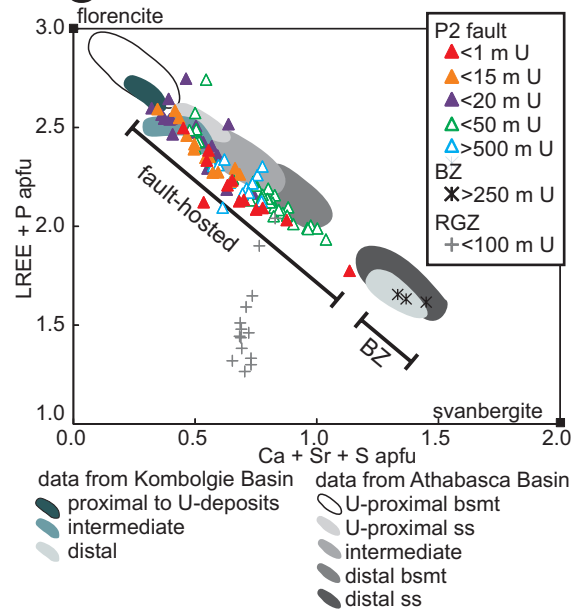


Figure 9



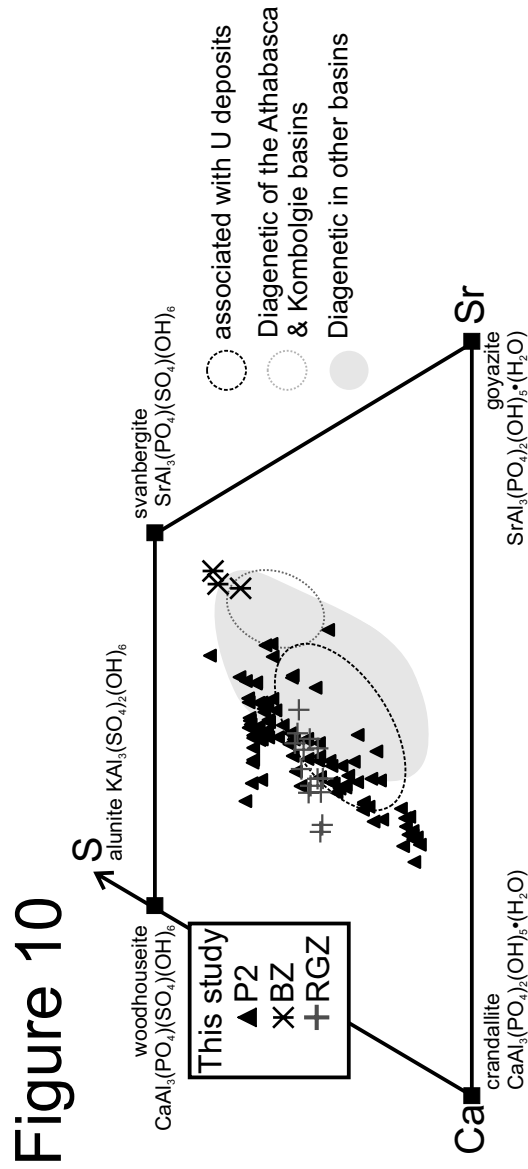


Figure 11

